

Contents lists available at ScienceDirect

Journal of Controlled Release

journal homepage: www.elsevier.com/locate/jconrel





Music enhances lipid nanoparticle brain delivery and mRNA transfection in brain cells[☆]

Patricia Mora-Raimundo ^{a,1,*}, Alon Gilon ^{b,1}, Haim Kadosh ^{a,c,1}, Yuval Richtman ^a, Mor Sela ^a, Shanny Ackerman ^a, Gal Chen ^{a,c}, Ravit Abel ^{a,d}, Shaked Kagan ^a, Noga Sharf-Pauker ^{a,d}, Or Gigi ^a, Hanan Abumanhal-Masarweh ^{i,j}, Utkarsh Tripathi ^e, Malak Saada ^e, Aviram Shemen ^e, Daphna Link-Sourani ^{g,h}, Jeny Shklover ^a, Rola Farah ^{f,g,h}, Tzipi Horowitz-Kraus ^{f,g,h}, Marilena Hadjidemetriou ^{i,j}, Kostas Kostarelos ^{i,j,k}, Shani Stern ^e, Avi Schroeder ^{a,*}

- ^a The Louis Family Laboratory for Targeted Drug Delivery and Personalized Medicine Technologies, Department of Chemical Engineering, Technion Israel Institute of Technology, Haifa 3200003, Israel
- ^b BPM College, Haifa 3303333, Israel
- ^c The Interdisciplinary Program for Biotechnology, Technion Israel Institute of Technology, Haifa 3200003, Israel
- d The Norman Seiden Multidisciplinary Program for Nanoscience and Nanotechnology, Technion Israel Institute of Technology, Haifa 3200003, Israel
- ^e Sagol Department of Neurobiology, Faculty of Natural Science, University of Haifa, Haifa 3498838, Israel
- ^f Educational Neuroimaging Group, Faculty of Education in Science and Technology, Technion, Israel
- g Faculty of Biomedical Engineering, Technion Israel Institute of Technology, Haifa 3200003, Israel
- h The May-Blum-Dahl MRI Research Center, Technion Israel Institute of Technology, Haifa 3200003, Israel
- i NanoOmics Lab, Division of Cancer Sciences, School of Medical Sciences, Faculty of Biology, Medicine and Health, The University of Manchester, Manchester, UK
- ^j Centre for Nanotechnology in Medicine, Faculty of Biology, Medicine and Health, The University of Manchester, Manchester, UK
- k Nanomedicine Lab, Catalan Institute of Nanoscience & Nanotechnology (ICN2) and Catalan Institute of Research and Advanced Studies (ICREA), Barcelona, Spain

ARTICLE INFO

Keywords: Lipid nanoparticles Music-driven nanomedicine Gene delivery Neurostimulation Auditory stimulation

ABSTRACT

Delivering therapeutic agents to the brain, particularly to neurons, is crucial for advancing treatments for neurological diseases. In this study, we introduce a non-invasive approach using music to enhance the delivery of lipid nanoparticles (LNPs) to the brain, potentially improving drug uptake. While LNPs have demonstrated significant potential in systemic delivery, various strategies have been explored to enhance their brain delivery. Here, we investigate the potential of audible sound waves, i.e., music, to enhance nanoparticle neuronal uptake and brain penetration. We tested different sounds across frequency ranges: low (10-250 Hz), mid (160-3800 Hz), high (1250-22,000 Hz) and a complex soundtrack of Pink Floyd "Another Brick in the Wall, Part 1" (128-5600 Hz). Low-frequency sound or soundtracks containing low frequencies in their spectrum (such as Pink Floyd) achieved significantly higher nanoparticle uptake in primary cortical neurons. Specifically, exposure of primary cortical neurons to low-frequency sound (10-250 Hz) enhanced LNP uptake and transfection in neuronal cultures, resulting in a 10-fold increase in gene expression. Low frequencies are often used for mechanical cellular stimulation, which may explain the effect of specific frequency ranges to achieve higher uptake and expression. In vivo, we found that mice that were administered with mRNA-LNP intravenously and exposed to audible lowfrequency sounds had higher mRNA expression in the brain compared to non-exposed mice, with gene expression localized in the midbrain and thalamus - key regions involved in sound processing and emotional regulation. Mass spectrometry analysis of mice plasma showed that sound stimulation modulates the abundance of proteins involved in cytoskeletal dynamics and cellular uptake. Additionally, low-frequency sound exposure modulated the immune responses in mice, reducing neutrophil count in the blood and potentially lowering inflammation markers following intravenous LNP administration. In healthy human volunteers, functional MRI demonstrated that exposure to low-frequency audible sound elicited frontal, temporal, and occipital brain activation, in addition to the activation of classical auditory brain regions. This work explores a non-invasive neuro-

[†] This article is part of a Special issue entitled: 'SPLC-CRS 2024 Conference' published in Journal of Controlled Release.

^{*} Corresponding authors.

E-mail addresses: patriciamora0111@gmail.com, patmora@campus.technion.ac.il (P. Mora-Raimundo), avids@technion.ac.il (A. Schroeder).

¹ These authors contributed equally to this work.

stimulatory method for therapeutic brain delivery, potentially opening new possibilities for precision medicine, where sound waves are tailored to activate specific brain regions, for targeted treatment of neurological disorders.

1. Introduction

Brain diseases, including neurodegenerative disorders such as Alzheimer's and Parkinson's, present a significant challenge in modern medicine [1]. One of the primary obstacles is the blood-brain barrier (BBB), a highly selective barrier that restricts the entry of many therapeutic agents into the brain [2]. In recent years, gene therapy has emerged as a promising approach for treating complex brain diseases, offering the possibility of correcting underlying genetic defects. Nucleic acids, including siRNA [3,4], mRNA [5], and DNA [6], are at the forefront of this therapeutic revolution. However, efficient delivery of such therapeutics across the BBB to their target sites within the brain remains a major challenge. Lipid nanoparticles (LNPs) have emerged as a leading platform for delivering nucleic acids, offering protection against degradation and facilitating cellular uptake [7,8]. These nanocarriers have shown potential in systemic gene therapy, as demonstrated by the recent success of mRNA vaccines [9]. However, their application for brain-targeted delivery remains limited due to the inherent challenges posed by the BBB and neuronal uptake. Various strategies have been explored to improve the delivery of LNPs to the brain. These include surface modifications with targeting ligands such as transferrin [6,10] and receptor-specific antibodies [11–14], which can guide nanoparticles to cross the BBB via receptor-mediated transcytosis. Additionally, physical methods like focused ultrasound (FUS, ultrasound is sound waves above 20 kHz, which are beyond human auditory ability) [15], in combination with microbubbles, have been employed to exert cavitational forces and thus transiently open the BBB successfully improving nanoparticle, including LNP brain delivery [15-18]. In an alternative therapeutic approach, ultrasound neuromodulation has been explored recently to modulate neuronal activity in the central nervous system [19,20]. FUS has been used for neuronal stimulation, exciting primary cortical neurons in culture through a mechanical mechanism mediated by specific calcium-selective mechanosensitive ion channels [21,22]. Other mechanical stimulations, such as pressure pulses, have shown potential to increase neuronal activity as well as differentiation [23,24]. Here, we hypothesized that through low-frequency audible sound wave stimulation of neurons we can modulate LNP cellular uptake. We propose a non-invasive approach using music (audible sound, sound waves in the range of 20 Hz - 20 kHz), to enhance LNP uptake. Sound, considered as a vibration that propagates as an acoustic wave through a transmission medium such as a gas, liquid, or solid, has been shown to influence neuronal activity and brain plasticity [25-33]. Music, as a combination of sounds used in a determined pattern, has been increasingly acknowledged as a potential therapeutic or rehabilitative tool, especially within the context of neurological and psychiatric disorders, recognizing its immense power to engage multiple brain systems, induce plasticity, etc. Some studies focused on the motor component, communication, memory, or cognition-driven psycho-emotional effects to improve patients' quality of life [34-38]. In addition to the beneficial effect of the music itself, we hypothesize that specific sound frequencies can enhance neuronal LNP uptake, offering a non-invasive and potentially region-specific method for brain-targeted drug delivery. In this work, we evaluated how different sounds affect LNP uptake and nucleic acid expression in primary neuronal cultures, achieving a 10-fold increase in overall protein expression, including contributions from supportive cells, when cells were exposed to low-frequency sound. More specifically, neuronal protein expression increased by approximately 40 % in response to sound exposure. After injecting LNPs intravenously to mice, sound exposure resulted in specific localization and a significant increase of protein expression, compared with non-sound exposed mice,

in the thalamus and midbrain - areas strongly associated with sound processing and emotions.

Furthermore, one of the adverse effects associated with mRNA-LNP administration is the activation of immune responses [39]. Specifically, complement activation, cytokine storms have been observed, where inflammatory cytokines such as interleukin (IL)-1β and IL-6 are excessively released, leading to systemic inflammation [40]. mRNA-LNP administration has also been linked to an increase in neutrophils as part of the body's inflammatory response [41]. Elevated neutrophils have been documented in both preclinical studies with mRNA-LNPs and in the context of mRNA vaccines. For example, after receiving the COVID-19 mRNA vaccine, some patients experienced higher neutrophil count, as part of a broader immune response that includes local inflammation and systemic effects such as fever, fatigue, or muscle aches [41]. While this inflammatory response is crucial for effective vaccine responses, it can sometimes result in adverse effects, particularly in individuals who experience a stronger-than-expected immune reaction or in patients requiring multiple injections for treatment of chronic diseases like neurological disorders [42]. We explored whether audible sound exposure modulates the immune response following LNP administration. Our findings show that sound exposure reduced blood neutrophil counts 48 h post-injection and affected IL-6 cytokine release, both of which are associated with inflammation in response to LNP administration. Sound exposure thus presents a promising approach to minimize adverse effects associated with LNP therapeutics. These findings highlight the potential of audible sound (including music) as an effective strategy for enhancing therapeutic delivery across the BBB, paving the way for new treatments for neurological disorders.

2. Materials and methods

2.1. Synthesis of Lipid Nanoparticles (LNPs)

2.1.1. DMG-PEG2000-glucose

The synthesis of DMG-PEG 2000-glucose was performed as previously stated [M. Sela; G. Chen et al. Unpublished results]. Shortly, d-Glucuronic acid (G5269; Sigma-Aldrich; 22.0 mg, 0.113 mmol) was dissolved in 1 mL DMF, and after we add EDC (23.9 mg, 0.125 mmol) and NHS (14.4 mg, 0.125 mmol). The reaction was stirred overnight at 4 °C under nitrogen atmosphere. D-Glucuronic-NHS (0.0756 mmol) was added to 0.45 ml chloroform and 0.5 ml DMF containing DMG-PEG2000-NH2 (50 mg, 0.0199 mmol) and triethylamine (67 μ l). The reaction was stirred overnight at 25 °C under nitrogen atmosphere. We purified the product by heptane precipitation, rotary evaporation, and dialysis. DMG-PEG2000-glucose was obtained after lyophilization and stored as 10 mM dry DMSO stock at -80 °C until use.

2.1.2. Synthesis of Lipid Nanoparticles (LNPs)

The formulation of particles was done as previously reported in our lab [M. Sela; G. Chen et al. Unpublished results]. Briefly, we used the microfluidic mixing method obtaining higher reproducibility, uniformity of LNPs, and precise control over mixing parameters [43].

We dissolved in ethanol a lipid mixture of SM-102 (2089251–47-6; Tzamal D-Chem Laboratories Ltd., Israel), DOPE (565,600; Lipoid, Germany) cholesterol (C8667; Sigma-Aldrich), (DMG-PEG1000) (001317-1 K; Biopharma PEG, USA) and DMG-PEG2000-glucose, in molar percentages of 50.25:10.05:38.19:1.01:0.5, (organic phase). To prepare untargeted-LNPs (LNPs-UT), we used DMG-PEG2000 (001317-2 K; Biopharma PEG, USA). 60 µg of the nucleic acid (mRNA) were dissolved in 10 mM citrate buffer (pH 4.5) to produce an aqueous phase.

Using the NanoAssembler Ignite (NIN0001; Cytiva, USA; provided by A. Zinger lab, Technion) the organic and aqueous phases were combined at a 1:5 volumetric ratio and 12 mL/min flow rate and diluted in a 1:1 volume ratio in PBS. LNPs were then dialyzed against PBS (pH 7.4; 1:1000 volume ratio) using a 3.5–5 kDa dialysis membrane (133,198; Repligen, USA) to change the organic solvent to a PBS buffer at 4 $^\circ$ C for 24 h.

2.1.3. Physical characteristics and encapsulation efficiency

The physical characteristics of LNPs, mean size diameter (nm), PDI, and zeta potential (mV), were measured using dynamic light scattering with a Zetasizer Ultra (Malvern, UK). To measure mRNA encapsulation efficiency, we conducted the Quant-iT RiboGreen RNA Assay K\1 kit (R11490; Thermo Fisher, Rhenium, Israel) following manufacturer protocol. LNPs were diluted 1:50 in either TE buffer or 1 % Triton X-100 (93,443; Sigma-Aldrich) in TE buffer, plated on a 96-well plate, and incubated at 37 °C for 10 min to induce lysis. RiboGreen reagent was then added to each well. After 5 min at 25 °C of incubation, the fluorescence intensity was measured on a plate reader (Tecan, Switzerland) at an excitation/emission of 485/528 nm. LNP mRNA encapsulation efficiency (%) was calculated by subtracting the unencapsulated mRNA fluorescence intensity value (intact LNPs in TE buffer) from total mRNA fluorescence intensity value (lysed LNPs in Triton X-100) and then divided by the total mRNA fluorescence intensity and multiply by 100.

2.2. Design of sound stimuli

To investigate the effects of sound on nanoparticle brain uptake, we designed a set of sound stimuli with varying frequency ranges. The sound stimuli were generated using Ableton's Wavetable synthesizer or *Operator*, employing wavetable synthesis techniques. Each soundtrack was modulated to span distinct frequency ranges to explore their potential differential impact.

Four types of sound stimuli were designed:

- Sound 1 (Nazare Copyright © 2024 Alon Gilon) is a modulated bass audio track characterized by a rich, textured quality that exhibits continuous pulses throughout its duration. Rough, fatty and with heavy tone, giving it a dense and unpolished feel. The sound generates continuous pulses at one-second intervals. The spectral centroid range (centre of mass): 10 Hz to 248 Hz (D#-2 to B2), with key frequencies including the fundamental frequency at 48 Hz (G0) and its fifth harmonic. The sound is notably rich in harmonics, while exhibiting a reduction in mid-high frequency range content due to an external filter. The overall frequency spectrum extends from 10 Hz to 22.1 kHz (D#-2 to 137 sm), with a filtered range of 181 Hz to 22.1 kHz. Sound 1 was synthesized using two oscillators, employing sine and square wave types. The amplitude characteristics of the sound are crucial for its perception and functionality within the experimental context. Its amplitude envelope follows an ADSR (Attack, Decay, Sustain, Release) pattern, meticulously crafted to shape the sound's dynamic profile over time. To enhance the complexity of the sound, modulations are applied via a square wave Low Frequency Oscillator (LFO), which modulates the oscillator 1 position (wave type), filter frequency 1, and pitch. Additional audio effects, including saturation, low-frequency enrichment and equalizer were incorporated to further enrich the sound.
- Sound 2 (Battersea Copyright © 2024 Alon Gilon) is a modulated bass audio track characterized by a flat and rough texture reminiscent of an old industrial machine, conveying a gritty atmosphere. It includes a consistent, periodic element a muffled knocking sound that repeats at intervals of less than a second. It was designed and synthesized using Ableton's Wavetable synthesizer, employing wavetable synthesis techniques. The spectral centroid range (centre of mass): 10 Hz − 239 Hz (D#-2 A#2), with key frequencies including the fundamental frequency at 20 Hz (D#-1), fifth harmonic

- and 1 octave (above fundamental). The sound is notably rich in harmonics, while exhibiting a reduction in mid-high frequency range content due to an external filter. The overall frequency spectrum extends from 10 Hz to 22.1 kHz (D#-2 to 137 sm), with a filtered range of 181 Hz to 22.1 kHz. Sound 2 was synthesized using two oscillators, employing sine wave type. The amplitude characteristics of the sound are crucial for its perception and functionality within the experimental context. Its amplitude envelope follows an ADSR pattern, meticulously crafted to shape the sound's dynamic profile over time. To enhance the complexity of the sound, amplitude modulation is applied via a square wave LFO, which modulates the amplitude (ADSR). Additional audio effects, including saturation, low-frequency enrichment and equalizer were incorporated to further enrich the sound.
- Sound 3 (Biarritz Copyright © 2024 Alon Gilon) is a mid-range sound with a plastic, hollow timbre that evokes tonal qualities reminiscent of soundscapes from 1990s computer games. Characterized by a wave-like motion, giving the impression of continuous upward and downward movement. The sound was designed and synthesized using Ableton's Wavetable synthesizer, employing both sawtooth and triangle waves modulated by pitch variation. The spectral centroid range (centre of mass) is 160 Hz - 3.79 kHz (D#2 to A#6), with key frequencies including the fundamental at 257 Hz (C3) and other dominant frequencies. The overall frequency spectrum covers 10 Hz to 10 kHz (D#-2 to D#8), with significant reductions in the low and high frequency ranges due to external equalization. The use of low-cut and high-cut filtering (10 Hz - 313 Hz (D#-2 to D#3), 3.03 kHz - 22.1 kHz (F#6 to 137sm)) and additional equalization further shapes the sound's texture, creating a refined yet synthetic aesthetic. Sound 3 was synthesized using two oscillators, employing, square wave (oscillator 1) and between sawtooth wave and triangle wave (oscillator 2) types. The amplitude envelope follows a precise ADSR pattern, with a minimal attack time and a short decay, leading to a sustained tone with a brief release. Pitch modulation is applied through a sine wave LFO, subtly altering the wave's motion at regular intervals of around 2 s.
- Sound 4 (Sierra Leone Copyright © 2024 Alon Gilon) is a high-frequency audio track, characterized by sharp, high-pitched tones that resemble a rubbing or shrill beeping noise. Its spatial movement creates a rotational sensation, enhancing its dynamic quality. Synthesized using Ableton's *Operator*, it employs frequency modulation synthesis. Its spectral centroid range (centre of mass) is 1.25 kHz to 21.7 kHz (D#5 to 136 semitones), with the fundamental frequency at 2.17 kHz (C#6). The overall frequency spectrum extends from 10 Hz − 22.1 kHz (D#-2−137 sm). A filtered ranges of 10 Hz − 1.63 kHz (D#-2 to G#5) and 21.6 kHz − 22.1 kHz (136sm to 137sm), focusing on its sharp, high-frequency elements. Sound 4 was synthesized using three oscillators, employing square wave, sawtooth wave and triangle wave types. A sine wave LFO modulates the oscillators, producing periodic rotational effects in the sound's spatial profile.
- Sound 5 is a 10-s excerpt from Pink Floyd's "Another Brick in the Wall, Part 1" spanning from 1:25 to 1:35in the original track. The sound is atmospheric, warm and spacious, with rich harmonics typical of the progressive rock genre. The section includes bass, ambient percussive guitar work, melodic guitar and reverb creating a spacious, meditative atmosphere. It contrasts with the more synthesized sounds used in the experiments, offering a complex blend of live instrumentation and studio effects. The spectral centroid range (centre of mass) is 128 Hz - 5.61 kHz (C#2 – F#7) rich in frequencies and sonic complexity, providing a different auditory texture compared to the synthesized sounds. Its musicality and production nuances offer a unique perspective in the investigation of sound's effects on nanoparticle brain uptake. The overall frequency spectrum extends from 10 Hz - 22.1 kHz (D#-2-137 sm). For experimental purposes, external equalization was applied with a low cut at 205 Hz and a high cut at 7.14 kHz, shaping the filtered range between 10 Hz

to 205 Hz (D#-2 to G#2) and 7.14 kHz to 22.1 kHz (A7 to 137 sm). These equalization settings highlight the essential frequencies in the mid-range, while eliminating extreme lows and highs to focus on the warm core of the sound. Additionally, a saturator effect was added to introduce subtle harmonic richness.

The synthesized sounds used in this study (referred to as Sound 1, Sound 2, Sound 3, and Sound 4) are original works created by Alon Gilon and are protected by copyright.

Sound files were played at an intensity of 80 dB SPL measured at a standard distance of 30 cm. The volume and duration were kept constant across all different soundtracks to ensure uniform exposure conditions. We used Yamaha powered speaker system, model HS7 (provided by Alon Gilon), while isolated from the surface, positioned at 30 cm form the experimental subject (LNPs sample, cells culture plate, mice cage), and the subject was lifted (if necessary) to stay aligned with the lower woofer. Calibration was performed using a sound level meter, Decibel X, to ensure consistent sound pressure levels across the experiments. The sounds were played for a total period of 2 h. During each 10-min interval, the sound was alternated: it was played for 10 s, followed by 10 s of silence, repeated throughout the 10 min. After each 10-min sound cycle, there was a full 10-min break with no sound when cells were placed back in the incubator (the same process of out and in for 10 min intervals from the incubator were performed in the cells that were not exposed to any sound to keep the same conditions). This pattern was repeated continuously for the entire 2- h duration. Sound characteristics are summarized in Table 1, and frequency spectrums and audio waveforms represent in Fig. S1.

2.3. Exposure of LNPs to sound stimuli and evaluation of mrna cargo release

LNPs were exposed to sound stimuli to evaluate the effect of acoustic waves on cargo retention and release. Specifically, LNPs were subjected to a low-frequency sound (Sound 1 and Sound 2), for a period of 2 h. The sound exposure protocol was identical to the one later used for cellular and animal experiments to ensure consistency (previously described). Following exposure, the release of the LNP cargo (mRNA) was evaluated by quantifying nucleic acid content in the supernatant. The nucleic acid release was first assessed using the Quant-iT RiboGreen RNA Assay K\1 kit (R11490; Thermo Fisher, Rhenium, Israel as described in the encapsulation efficiency evaluation.

2.3.1. Agarose gel electrophoresis

In addition, the integrity and release of RNA were analysed using agarose gel electrophoresis. LNPs were incubated with 1 % Triton X-100 to induce cargo release. Released RNA samples, intact LNPs, and LNPs exposed to Sound 1 and Sound 2 were mixed with loading dye and subjected to electrophoresis on a 1 % agarose gel containing ethidium bromide. Gels ran at 100 V for 45 min and visualized using a UV transilluminator. The gel images showed the absence of RNA bands, indicating no release from the LNPs following sound exposure.

Table 1 Synthesized sounds characteristics.

Sound Filter Name Description Synthesizer Oscillator wave Frequency range 181 Hz - 22.1 kHz Wavetable 10 Hz - 248 Hz Nazare © 1 Pulses, Rough, Heavy tone Sine and Square Battersea © 2 Flat, Rough, Consistent Wavetable 10 Hz - 239 Hz 181 Hz - 22.1 kHz Sine 10 Hz - 313 Hz and Biarritz © 3 160 Hz - 3.79 kHz Plastic, Hollow timbre Wavetable Square Sawtooth Triangle 3.03 kHz - 22.1 kHz 10 Hz - 1.63 kHz and Operator Sierra Leone © Sharp, high-pitched tones 1.25 kHz - 21.7 kHz Square Sawtooth Triangle 21.6 kHz - 22.1 kHz 10 Hz to 205 Hz and Pink Floyd 5 Atmospheric, Warm, Rock 128 Hz - 5.61 kHz 7.14 kHz to 22.1 kHz

2.4. LNPs surface charge in biological conditions

To assess the stability of lipid nanoparticles (LNPs) in biological conditions, particle testing in mouse serum was performed. Serum was diluted 2-fold in a 10 % sucrose solution. Equal volumes of the diluted serum and LNPs were mixed and incubated at 37 $^{\circ}\text{C}$ for 15 min. After incubation, an equal volume of 10 % sucrose solution was added to the mixture. The samples were centrifuged at 15,300 g for 1 h at 4 $^{\circ}\text{C}$, followed by two washes with 1× PBS for 5 min each. The final pellet was resuspended in 10 % sucrose solution and zeta potential was evaluated.

2.5. Cell culture

Each cell line was cultured at 37 °C in a humidified atmosphere containing 5 % CO₂, and a fresh medium was added every 2–3 days.

HEK 293 T cells, a human embryonic kidney cell line, were cultured under standard conditions. Cells were maintained in Dulbecco's Modified Eagle's Medium (DMEM) (D5796; Sigma-Aldrich), supplemented with 10% (ν/ν) fetal bovine serum (FBS) and with 1% (ν/ν) penicillin (10,000 units/ml), streptomycin (10 mg/ml; Pen-Strep) (030311B; Biological Industries, Israel) to prevent bacterial contamination.

hCMEC/D3 immortalized human brain capillary endothelial cells (Merck, USA) were provided by A. Sosnik (Laboratory of Nanomaterials Science, Department of Materials Science and Engineering, Technion). Cells (adherent) were cultured in EndoGRO-MV Complete Media Kit (SCME004; Merck Millipore, USA), supplemented with 1 ng/mL FGF-2 (GF003; Merck Millipore). Cell plating was performed on a flask coated with collagen type I, rat tail (08115; Merck Millipore) solution in PBS (BSS-1005-B; Merck Millipore) at a dilution of 1:20 and then incubated for 1 h at 37 °C. Then, trypsin-EDTA (SM2003C; Merck Millipore) was used for cell dissociation.

SH-SY5Y (ATCC), a thrice-cloned subline of the neuroblastoma cell line SK-N-SH, was provided by Prof. A. Fishman (Laboratory of Molecular and Applied Biocatalysis, Faculty of Biotechnology and Food Engineering, Technion). Cells (adherent) were cultured in a complete media comprising a 1:1 mixture of Dulbecco's Modified Eagle's Medium (DMEM) (D5796; Sigma-Aldrich) and Nutrient Mixture F12 HAM with sodium B (N4888; Sigma-Aldrich), supplemented with 1 % (ν / ν) penicillin (10,000 units/ml), streptomycin (10 mg/mL; Pen-Strep) (030311B; Biological Industries, Israel), 1 % (ν / ν) amphotericin B (Amp—B; 2.5 mg/mL) (030281B; Biological Industries), 10 % (ν / ν) FBS, and 1 % (ν / ν) non-essential amino acids (013401B; Biological Industries). In general, cells were dissociated and harvested using a cell scraper.

For neuronal differentiation, SH-SY5Y cells were seeded on 1 % gelatin from porcine skin, gel strength 300, Type a (G2500; Sigma-Aldrich) coated plates, followed by incubation in complete media supplemented with 10 μM all-trans retinoic acid (RA) (R2625; Sigma-Aldrih) for 4 days. Then, the medium was replaced with a starvation media (complete media without FBS), supplemented with 50 ng/ml human BDNF factor (4500210; PeproTech, Israel) for an additional 4 days; the cells were fully differentiated after 7 days.

Primary cortical neurons, all primary neurons extractions were

approved by the Inspection Committee on the Constitution of the Animal Experimentation at the Technion (IL1161020) and conducted according to its stipulated regulations. Cultures of primary neurons were established as previously stated [44,45]. Briefly, extracted rat neonates (P0) brain cortex were dissociated and plated onto 12 mm polyD-lysine (Sigma-Aldrich, Cat. #P6407)- treated glass coverslips. Cultures were then maintained in an enriched growth media and grown at 37 $^{\circ}\text{C}$ and 5 % CO2. Following five days in-vitro, growth medium was supplemented with 4 μM cytosine-arabinoside (ARA—C) to suppress glia proliferation. Experiments were performed between 8 and 10 days in vitro.

2.6. In vitro sound exposure cell viability

Cells were exposed to the specific sound for 2 h, following the previously described protocol. Sixteen hours after sound exposure, a cell viability test was performed using the PrestoBlue assay (A13261; Thermo Fisher, USA), according to the manufacturer's instructions. Ninety minutes after adding the reagent to the wells, the fluorescence signal (excitation: 535 nm; emission: 590 nm) was measured using a microplate reader. Fluorescence readings from the media-only control group were averaged and subtracted from all other values. The results for each treatment group were then normalized to the values of the untreated control group.

2.7. In vitro sound exposure LNPs transfection efficiency

To evaluate the influence of low-frequency sounds on LNP uptake and expression of encapsulated mRNA, different frequency ranges were tested in primary cortical neurons. The neurons were treated with 200 ng of luciferase mRNA-loaded LNPs (L-7202; Trilink BioTechnologies, US). Immediately after LNP treatment, the cells were exposed to Sounds 1–5, following the previously described sound exposure protocol. Sixteen hours after sound exposure, luciferase expression was measured. For this, 20 μ L of ONE-Glo Luciferase Assay System (E6110; Promega, US) was added to the media. The luminescent signal was then measured using a microplate reader. The luminescence Fluc photons/s obtained from LNPs were normalized against LNPs-UT without sound exposure (LNPs-UT NS).

To evaluate how different cell lines respond to sound exposure, sounds 1 and 2 were also tested on several cell lines. HEK 293 T cells and hCMEC/D3 cells were seeded (65,000 cells/mL) one day before the experiment. SH-SY5Y cells were seeded (65,000 cells/mL) and differentiated one week before the experiment. On the experiment day, cells were treated at a dose of 200 ng luciferase mRNA-LNPs (both untargeted and glucose modified) Immediately after LNP treatment, the cells were exposed to Sounds 1 and 2, following the previously described sound exposure protocol. Sixteen hours after sound exposure, luciferase expression was measured. To measure luciferase expression, 20 ul of ONE-Glo Luciferase Assay System was added to the media. Finally, the luminescent signal of the plates was measured using a microplate reader. The luminescence Fluc photons/s obtained from LNPs were normalized against LNPs-UT NS.

2.8. In vitro electrical stimulation

For biphasic square-wave electrical stimulation of cells, we developed a dedicated stimulation system. In this setup, platinum electrodes were attached to the covers of 24-well plates, with two electrodes positioned in each well. Each electrode consisted of two twisted platinum wires, 2 cm long and 0.25 nm in diameter (Alfa Aesar, U.K.), spaced 1.3 cm apart. These electrodes were connected to a signal generator (MULTICOMP PRO MP750510 – PRO), which allowed for precise control of stimulation parameters, including frequency and voltage for each application.

To evaluate how different cell lines respond to electrical stimulation, a frequency of 1 Hz was tested under increasing voltage values (80, 120,

and 160 mVpp). Primary neurons were seeded at a density of 200,000 cells/ml seven days prior to the experiment. SH-SY5Y cells were seeded at a density of 65,000 cells/ml and differentiated for one week before the experiment. On the day of the experiment, cells were treated with a dose of 200 ng of luciferase mRNA-LNPs (both untargeted and glucose modified). Immediately after LNP treatment, the cells were electrically stimulated three times for 30 s with 90 s intervals under the specified conditions with gaps of 8 min without any stimulation for a total period of 30 min. Sixteen hours later, a cell viability test was performed using the PrestoBlue assay as described previously, and luciferase expression was measured. To measure luciferase expression, 20 μ L of the ONE-Glo Luciferase Assay System was added to the media. Finally, the luminescent signal of the plates was measured using a microplate reader. The luminescence obtained from LNPs was first normalized to cell viability values (presto blue) and finally normalized against the LNPs-UT.

2.9. Microscopy imaging for evaluating cell transfection

For the live imaging experiments, confocal microscopy (LSM 710; Zeiss, Germany) was performed to examine LNPs uptake and mRNA expression primary neurons (Fig. 3C) and hCMEC/D3 cells (FigureS3A). Primary neurons were seeded (70,000 cells/well) in 96 well plate coated with polyD-lysine (Grenier Bio One, 655946). Eight days after primary cells seeding, cells were treated with 200 ng of mCherry mRNA-loaded LNPs-G, and immediately after exposed to sound 1 or 2 for 2 h. The following day, the medium was removed, and the cells were washed ($2\times$ with PBS), fixed (4 % PFA for 10 min), permeabilized (0.25 % Triton X100), blocked (5 % Normal Goat Serum [S-1000; Vector Laboratories Inc., USA] and immunostained with Rabbit Monoclonal Anti-b-IIItubulin (1:1000) (ab18207; Abcam) and Goat Anti-Rabbit Alexa Fluor 488 (1:500) (ab150077, Abcam); the cells were stained with Hoechst (1 $\mu gmL{-}1)$ for nuclei labeling. Imaging was performed (LSM 710; Zeiss, Germany) at the LSE Infrastructure Center (Technion). The acquisition was performed using ZEN software with 405-, 488-, and 543 lasers.

The images were analysed using the IMARIS software, allowing semiautomated tracing of Tdtomato expression with neuronal marker, along with the percentage of cells transfected from the region of study. The examined parameters and statistics were measured for at least 10 fields of two independent repetitions.

hCMEC/D3 cells were seeded (65,000 cells/ml) one day before the experiment. Cells were treated with 200 ng of mCherry mRNA-loaded LNPs-G, and immediately after exposed to sound 1 or 2 for 2 h. The following day, the medium was removed, and the cells were washed (2× with PBS), fixed (4 % PFA for 10 min), permeabilized (0.25 % Triton X100), blocked (5 % Normal Goat Serum [S-1000; Vector Laboratories Inc., USA] the cells were stained with Hoechst (1 μ gmL-1) for nuclei labeling. Imaging was performed by Lionheart FX automated microscope (BioTek, Santa Clara, CA).

2.10. Calcium imaging

Primary rat neurons were cultured on 18 mm glass coverslips and allowed to grow for 10 days in vitro (DIV) to reach maturity. The cells were loaded with [Calcium Indicator Dye, Fluo-4 AM] at a final concentration of 4 μM and incubated at 37 $^{\circ} C$ for an hour in a dark, humidified chamber. After washing to remove excess dye, the coverslips were mounted in a recording chamber with HEPES-based artificial cerebrospinal fluid (ACSF) containing NaCl (139 mM), HEPES (10 mM), KCl (4 mM), CaCl2 (2 mM), p-glucose (10 mM), and MgCl2 (1 mM), at pH 7.4 and osmolarity adjusted to 310 mOsm at room temperature. Imaging was performed using a Leica fluorescence microscope equipped with a (20× objective) and a high sensitivity sCMOS camera.

2.10.1. Experimental design

The neurons were exposed to three experimental conditions: (1) Before Sound, (2) During Sound, and (3) After Sound. For sound

stimulation, sound was applied for 10 min. Calcium imaging was recorded at a frame rate of 10 Hz for a total duration of 5–10 min per condition. Each experimental condition was repeated across 4 independent wells.

2.10.2. Data acquisition and preprocessing

Time-series images were acquired using Leica software and saved in TIFF format for further processing. Regions of Interest (ROIs) were identified automatically using a custom MATLAB script for neuronal detection. The calcium imaging data consisted of time-lapse sequences of fluorescence microscopy images capturing neuronal activity over time. Each frame represented the fluorescence intensity at a specific time point, reflecting variations in intracellular calcium levels, which served as a proxy for neuronal activity.

To extract ROIs representing individual neurons, we employed a custom MATLAB script for automated detection. First, all time-lapse frames were averaged to create a composite intensity map, consolidating temporal data into a single representative image. This process enhanced the signal-to-noise ratio and highlighted persistent features, such as neuronal bodies. Candidate ROIs were identified as local intensity maxima above a predefined percentile threshold, focusing on the brightest regions likely to correspond to neurons. To eliminate redundancy, a filtering step was applied to remove duplicate ROIs based on spatial proximity (<50 pixels) and signal correlation (>0.9). This ensured that each ROI corresponded to a unique neuron. Detected ROIs were validated visually by overlaying their positions on the composite image.

The raw fluorescence intensity (F) was processed to calculate the change in fluorescence ($\Delta F/F0$), where F0 represents the baseline fluorescence intensity for each ROI, determined by detrending the signal using the convex envelope method. This method effectively captured the overall trend and eliminated slow changes in the baseline. After detrending, a uniform filter with a window of 51 frames was applied to further reduce background noise. The detrended signal was then normalized by dividing by the convex envelope to produce the $\Delta F/F0$ ratio, minimizing effects of gradual fluorescence changes.

Calcium transients were detected by identifying peaks in the $\Delta F/F0$ signal that exceeded a threshold of 1.005. To ensure meaningful peaks were captured, a minimum distance of 40 frames was enforced between consecutive peaks, and a prominence threshold was applied to filter out insignificant peaks. Detected peaks were further consolidated by merging overlapping peaks based on spatial proximity (allowing a gap of up to 40 points) and signal properties (such as peak height). Consolidation ensured that each retained peak was distinct, minimizing artifacts and enhancing the reliability of detected neuronal activity. This peak detection technique follows a similar approach to that described in our previous work [46], ensuring consistency and robustness in identifying calcium transients. Additional parameters, such as rising and falling times were also calculated to characterize the temporal dynamics of each peak.

2.10.3. Analysis and metrics

For each ROI, we extracted several key metrics:

- Peak Frequency: Calculated as the number of detected calcium transients (peaks) divided by the total recording duration, providing a measure of how frequently calcium signaling events occurred.
- Area Under the Curve (AUC): For each detected transient, the AUC
 was calculated by integrating the ΔF/F0 signal over the duration of
 the event, giving an indication of the overall magnitude of calcium
 activity.
- Fraction of Active Time: Determined by summing the widths of all
 detected peaks for each ROI and dividing by the total recording time,
 this metric represented the proportion of time during which each
 neuron was active.

These metrics allowed us to quantify the frequency, magnitude, and duration of calcium signaling events, providing a comprehensive assessment of neuronal activity under each experimental condition.

2.11. Statistical analysis

The analysis was conducted on automatically marked ROIs. The top 10 most active ROIs were selected for visualization purposes to provide a representative depiction of neuronal activity under each condition. However, for statistical analysis, all detected ROIs were included to ensure a comprehensive data evaluation. Peak frequency, active time fraction, and average area under the curve were compared across conditions (Before Sound, During Sound, After Sound) using repeated measures one-way ANOVA. Significance was set at p < 0.05.

2.12. Mass spectrometry analysis of plasma samples

2.12.1. Sample preparation

Plasma samples (n=6) collected from control mice (males and females) and an additional set of n=6 samples collected from Sound 1exposed mice (males and females) were proteomically analysed using the Nano-omics workflow, as previously described. [47–50] Briefly, liposomal nanoparticles were incubated with plasma samples and purified using size exclusion chromatography and membrane ultrafiltration. Proteins adsorbed to the surface of the nanoparticles were quantified using the BCA Protein Assay Kit, following the manufacturer's instructions (Sigma (UK)).

For mass spectrometry analysis, 10 µg of total protein from each sample was mixed with 10 µL of lysis buffer (50 mM TEAB with 5 % SDS) and incubated at 4 °C for 1 h. The lysed samples were reduced with 5 mM dithiothreitol (DTT) and incubated at 60 °C for 10 min, followed by alkylation with 30 mM iodoacetamide (IAA) and incubation in the dark for 30 min. IAA was then quenched by the addition of DTT, and the solution was cleared by centrifugation at 14,000 $\times g$ for 10 min. The cleared supernatant was transferred to a fresh tube and acidified by adding phosphoric acid to a final concentration of 1.2 % (w/v). S-trap binding buffer (90 % methanol in 100 mM TEAB, pH 7.1) was added to increase the sample volume by six-fold. The samples were then transferred to the S-Trap $^{\text{TM}}$ micro spin columns (ProtiFi) and washed once with a methyl tert-butyl ether (MTBE)/methanol (10:3 v/v) solution, followed by three washes with the S-trap binding buffer. In-column digestion was performed by adding trypsin (1 μg trypsin in 20 μL) and incubating at 47 °C for 1 h. The resulting peptides were eluted and subsequently desalted in a 96-well filter plate with a $0.2~\mu m$ PVDF membrane (3504, Corning) using Oligo R3 resin beads (1-1339-03, Thermo Fisher Scientific), followed by two washes with 0.1 % formic acid. Peptides were finally eluted with 0.1 % formic acid in 30 % acetonitrile and lyophilized using a SpeedVac vacuum concentrator (Thermo Fisher Scientific).

2.12.2. Mass spectrometry and data analysis

Digested samples were analysed by liquid chromatography-tandem mass spectrometry (LC-MS/MS) at the Biological Mass Spectrometry Core Research Facility at the University of Manchester. The separation was performed on a Thermo RSLC system, which included a NCP3200RS nano pump, WPS3000TPS autosampler, TCC3000RS column oven, and an analytical column (Waters nanoEase M/Z Peptide CSH C18 Column, 130 Å, 1.7 μ m, 75 μ m \times 250 mm). The mobile phase consisted of buffer A (0.1 % formic acid in water) and buffer B (0.1 % formic acid in acetonitrile). A multistage gradient was applied, varying the percentage of buffer B as follows: 1 % to 6 % B over 2 min, 6 % to 18 % B over 44 min, 18 % to 29 % B over 7 min, and 29 % to 65 % B over 1 min. The gradient was followed by a 4-min wash at 65 % B. The gradient was then reduced to 2 % B over 1 min. The analytical column was connected to a Thermo Exploris 480 mass spectrometer via a Thermo nanos-pray Flex Ion source. Fragmentation data were obtained from ions with a charge

state of +2 or +3 and an intensity greater than 5000. These ions were dynamically excluded from further analysis for 15 s after a single acquisition within a 10 ppm window.

Raw mass spectrometry data were processed using Progenesis QI for Proteomics software (v. 3.0; Nonlinear Dynamics). RAW files were imported into the software, where automatic feature detection was performed. After selecting the reference run, all other runs were aligned to this reference. Automatic processing with specified filters was applied, including a maximum charge of 5 for peak charge, relative quantification using the Hi-N method, and the requirement of 3 peptides per protein. The resulting MS/MS peaks were exported and searched against the house mouse (Mus musculus) proteome from the UniProt database using a local Mascot server (v. 2.3.0; Matrix Science). The search parameters included oxidation of methionine (M) as a variable modification and carbamidomethylation of cysteine (C) as a fixed modification, with trypsin digestion and allowance for one missed cleavage. Peptides with charge states of +2 and +3 were considered, with a precursor mass tolerance of 20 mmu and a fragment mass tolerance of 5 ppm. The ESI-QUAD-TOF instrument was used for analysis. The generated XML file was imported into Progenesis QI v3.0 to map peptides to features, with a peptide spectrum match (PSM) score > 20. A 1 % false discovery rate (FDR) filter was applied to all significant PSM matches (*p*-value <0.05). Pairwise comparisons between the control and Sound 1 groups were performed using one-way ANOVA analysis, with the experimental designs set as "between subject" for the statistical analysis. The resulting protein lists, including one-way ANOVA p-values, q-values, maximum fold changes, and normalized protein abundances, were exported from Progenesis and further analysed using Excel (Microsoft), R (v. 4.2.2), and RStudio (v. 2023.06.0, PositSoftware).

The mass spectrometry proteomics data have been deposited to the ProteomeXchange Consortium via the PRIDE partner repository with the dataset identifier PXD067827 and 10.6019/PXD067827

2.12.3. Pathway analysis using Integrative Pathway Analysis (IPA)

Ingenuity Pathway Analysis (IPA) (Qiagen) was used to identify and analyse enriched biological pathways associated with the differentially abundant proteins (DAPs) identified between control and Sound 1 exposed groups. The DAPs, along with their corresponding p-values and maximum fold changes, were imported into IPA for pathway analysis. The IPA pathway analysis was conducted to identify the most relevant canonical pathways, upstream regulators, and molecules involved in the biological processes associated with the DAPs. From this analysis, pathways with significant log p-values were identified and exported. Subsequently, graphical representations of the top 10 enriched pathways with gene-ratio values, were created using R (v. 4.2.2), and RStudio (v. 2022.12.0, Posit Software). The data were visualized through bar plots and pathway network plot to highlight the key pathways altered in the study.

2.13. In vivo Cre mRNA delivery

All animal experiments were approved by the Inspection Committee on the Constitution of the Animal Experimentation at the Technion (IL0290123, IL1961124 and IL0070125) and conducted according to its stipulated regulations.

Females or Males Ai9 mice were obtained from an institutionally managed animal colony and at 10 weeks old they were dosed intravenously with LNPs encapsulating mRNA encoding Cre Recombinase (L-7211; Trilink BioTechnologies, US; 1 mg/kg). Immediately after, mice were exposed to sound 1 for a period of 2 h following the same sound protocol as used in the in vitro studies. After 2 days, the mice were sacrificed and perfused with either only PBS or with PBS followed by 4 % PFA in PBS. The brains were then extracted for further processing. Blood was collected for further analysis and other organs such as liver, kidney, spleen, lungs, hearth and ovaries were harvested. Mice non exposed to sound 1 after LNPs injection were used as control.

2.14. IVIS imaging

Biodistribution was performed using IVIS imaging. Except for the brains, extracted organs were imaged ex vivo at an excitation of 570 nm and emission of 620 nm, binning of 8, and f-stop of 2, with 5-s (except of liver 1-s) exposure time for tdTomato mRNA expression detection (Fig. S6, Supporting Information). Ex vivo brain images were obtained at an excitation of 570 nm and emission of 620 nm, binning of 8, and f-stop of 2 and 5-s exposure time parameters. Quantitative data from all images were analysed using the ROI tool in Living Image software. A control (non-injected) mouse was used for analysis, with average radiance subtracted from the average radiance of each injected tissue, respectively.

2.15. Fluorescence immunohistochemistry analysis

Fluorescence immunohistochemistry was employed to visually confirm the tdTomato expression of LNPs throughout the entire brain. The Ai9 mice 10 weeks old received an intravenous injection of LNPs-G encapsulating Cre mRNA (1 mg/kg) and afterwards immediately exposed to sound 1 for a period of 2 h. Two days later, the mice were anesthetized, sacrificed, perfused with ice-cold PBS followed by 4 % PFA in PBS, and their brains were collected for the fluorescence immunohistochemistry process. Untreated mice served as the control group.

The brains were postfixed for ON in 4 % PFA, washed twice with PBS, and then cryoprotected by 30 % sucrose in PBS at 4 $^{\circ}$ C for 2–3 days. After cryoprotection, the brains were embedded in the O.C.T. compound (BN62550; Bar-Naor, Israel), frozen, and then stored at $-80~^{\circ}$ C until further processing. The brain sections were obtained by a cryostat machine. The slices sectioned on the coronal plane at 50 μm , mounted with DAPI fluoromount-G (010020; ENCO, Israel), covered-slipped, and dried overnight at 4 $^{\circ}$ C. The slides were imaged the following day using Bio-Rad ChemiDoc under cy3 filter 27-s exposure (Green Epi Illumination, emission 602/50 Filter) and colorimetric 0.2-s exposure (White Epi Illumination, emission 590/110 Filter).

2.16. Hematology blood test

Blood samples were collected from mice 48 h after LNPs administration and sound exposure. The mice were sacrificed and terminally bled through a cardiac puncture. To analyse the chemistry parameters, blood samples were incubated on ice for 30 min, followed by centrifugation for 10 min at 10000 rpm to separate the serum. A heparin-coated syringe was used to collect blood samples into EDTA-covered vials to prevent clot formation. An analysis of blood cell counts and ELISA cytokine test was conducted (American Medical Laboratories, Israel) to evaluate the potential systemic immunogenicity and inflammation of LNPs treatment and the potential beneficial effect of music. All values were normalized to the healthy control group.

3. fMRI experimental design and sound exposure protocol

3.1. Participants

Four healthy adults (2 women, 2 men), aged 28 to 49 years (mean age $=37, \mathrm{SD}=10.23$), participated in the current study. All participants were monolingual native Hebrew speakers. Written informed consent was obtained from all patients, and prior to the start of the study, approval was granted by the Institutional Review Board and Human Subjects Protection (US-HHS-FWA-00013345), The Ruth and Bruce Rappaport Faculty of Medicine, Technion - Israel Institute of Technology (approval number: 188–2024).

3.1.1. Study procedure

The following inclusion criteria were applied: (1) healthy adults, (2) normal or corrected-to-normal vision and hearing, (3) no history of

psychiatric or neurological disorders, (4) non-verbal IQ above 85, and (5) no contraindications for MRI scanning, such as claustrophobia or the presence of metal implants (e.g., cardiac pacemakers, dental braces, or cochlear implants). The study protocol was approved by the Institutional Review Board, and data collection was conducted at the Technion Human MRI Research Center (TecHMRC), Department of Biomedical Engineering, Technion - Israel Institute of Technology, Haifa, Israel.

3.1.2. Neuroimaging tasks

In line with the previously described study conditions, participants completed three separate fMRI audio-based tasks: (1) the Pink Floyd condition (frequency range: 128–5610 Hz) (Sound 5), (2) the Sierra Leone condition (frequency range: 1250–21,700 Hz) (Sound 4), and (3) the Nazareth condition (frequency range: 10–248 Hz) (Sound 1). All auditory stimuli were delivered using OptoActive earplugs (Optoacoustics LTD), which attenuate MRI scanner noise by 30–40 dB while maintaining high-fidelity audio transmission, particularly important for lower frequency sounds.

Each task was presented separately in a randomized order, using a block design. For each condition, participants listened to five undisturbed audio recordings. Each recording began with a 30-s silent control period, followed by 30 s of task-specific audio. Participants were instructed to remain attentive to the sounds and to keep their eyes open throughout the session.

3.1.3. Neuroimaging data acquisition

Prior to scanning, participants underwent a desensitization procedure to familiarize them with the MRI environment in a comfortable and supportive manner. This included practicing lying still on the scanner bed to minimize motion during the scan. To further reduce head movement, elastic bands were used to stabilize the head within the coil.

Functional MRI scans were conducted using a 3 T Siemens Prisma MRI system (Siemens Healthineers, Erlangen, Germany) equipped with an audiovisual presentation system (Psychology Software Tools, Pittsburgh, PA, USA) and a 64-channel head-neck coil for neuroimaging data acquisition.

Anatomical images were acquired using a T1-weighted MPRAGE pulse sequence, with a spatial resolution of $1\times1\times1$ mm 3 . Functional images were obtained using a T2*-weighted echo-planar imaging (EPI) sequence with the following parameters: repetition time (TR) = 1000 ms, echo time (TE) = 30 ms, flip angle = 68°, and voxel size = $2\times2\times2$ mm 3 . Each functional volume consisted of 306 frames, with each slice being 2 mm thick.

3.1.4. Data preprocessing

Functional MRI data were processed using SPM12 (Wellcome Trust Centre for Neuroimaging, UK) [1]. Preprocessing steps included realignment (using three translational and three rotational parameters), coregistration of the anatomical image to the mean realigned functional image, tissue segmentation, normalization to the Montreal Neurological Institute (MNI-152) template, and spatial smoothing using a Gaussian kernel (full-width at half-maximum, FWHM) of 2×3 mm.

Following first-level analysis and condition definition (audio vs. silence blocks), a second-level group analysis was performed to compute the average activation patterns for each of the three auditory tasks across the four study participants. Statistical results were corrected for multiple comparisons using family-wise error (FWE) correction at p < 0.05.

3.2. Statistical analysis

All data were reported as the mean \pm SD. Comparisons were performed between distinct groups. Groups were analysed by a two-tailed unpaired t-test, one-way analysis of variance (ANOVA), and two-way ANOVA. Statistical significance was set as *p < 0.05, **p < 0.01, ***p < 0.001, and ****p < 0.0001, with a 95 % confidence interval.

Analysis and figures were generated using GraphPad Prism v. 8.0 (GraphPad Software, Inc., La Jolla, CA, USA).

4. Results and discussion

4.1. Design of sound stimuli battery

To investigate the effects of sound on nanoparticle brain uptake, we designed a set of sound stimuli with varying frequency ranges. Each soundtrack was tailored to focus on distinct frequency ranges to assess its unique impact (Fig. 1A, Table 1). Although all sounds included a broad range of frequencies, they were filtered to emphasize a specific frequency range with the highest amplitudes within that range (Fig. S1 Supporting Information). Nazare (Sound 1) features a rich, textured bass track with a frequency range from 10 Hz to 248 Hz, utilizing sine and square wave oscillators. It is characterized by continuous one-second pulses (isometric repetition) creating a dense, unrefined sound resembling a beat (Fig. S1A i, ii Supporting Information). Battersea (Sound 2) presents a gritty, industrial texture, synthesized from sine waves with a spectral range of 10 Hz to 239 Hz and a periodic muffled knocking sound that repeats at intervals of less than a second giving a sense of pulse or beat, enhancing its mechanical atmosphere (Fig. S1B i, ii Supporting Information). Biarritz (Sound 3) has a hollow, synthetic timbre created with sawtooth and triangle waves, and features a frequency range from 160 Hz - 3.79 kHz, shaped by low and high cut filters. Its wave-like motion instills a sense of continuous movement (Fig. S1C i, ii Supporting Information). Sierra Leone (Sound 4) delivers sharp, high-pitched tones resembling beeps, synthesized using frequency modulation with a range of 1.25 kHz to 21.7 kHz, producing a dynamic rotational quality (Fig. S1D i, ii Supporting Information). Lastly, Pink Floyd (Sound 5) is a 10-s excerpt from Pink Floyd's "Another Brick in the Wall, Part 1", showcasing a rich harmonic texture with a frequency range of 128 Hz to 5.61 kHz. This sound contrasts with the synthesized tracks, offering a warm, meditative ambiance enhanced by external equalization to highlight essential mid-range frequencies (Fig. S1E i, ii Supporting Information). The synthesized sounds used in this study (referred to as Sound 1, Sound 2, Sound 3, and Sound 4) are original compositions created by Alon Gilon and are protected by copyright.

4.2. Design and physicochemical characterization of glucose-functionalized LNPs

The lipid nanoparticles (LNPs) used in this study are composed of four main components: an ionizable lipid, a phospholipid, cholesterol, and a PEG-lipid. The ionizable lipid SM-102, an FDA-approved lipid [51], becomes positively charged under acidic environments [52], enhancing nucleic acid encapsulation and promoting endosomal escape [52]. This LNP composition, previously described in our lab, has demonstrated successful brain uptake and cellular mRNA transfection [53]. The PEG-lipid prolongs circulation time, enhances delivery efficiency by reducing aggregation, opsonization, and phagocytosis [52,54]. Our previous work also demonstrated that PEG molecules facilitate enhanced neuronal uptake of liposomes [55,56]. The choice of phospholipid is important for efficient nucleic acid delivery, and DOPE was selected as phospholipid component due to its superior ability to promote endosomal escape compared to DSPC-based formulations [57].

To further improve targeting efficiency, we chemically modified 1,2-dimyristoyl-rac-glycero-3-aminepolyethylene glycol-2000 (DMG-PEG2000-NH2) with glucose, following a previously established method [58]. This modification attaches the targeting moiety to the amineterminated group of the PEG-lipid, preserving the standard LNP properties. Glucose was selected as the targeting agent due to its potential to interact with glucose transporters on brain endothelial cells [59], which are key components of the blood-brain barrier (BBB) [60], as well as neurons [59] (Fig. S2A Supporting Information).

The LNPs were engineered using microfluidic mixing [61] of an

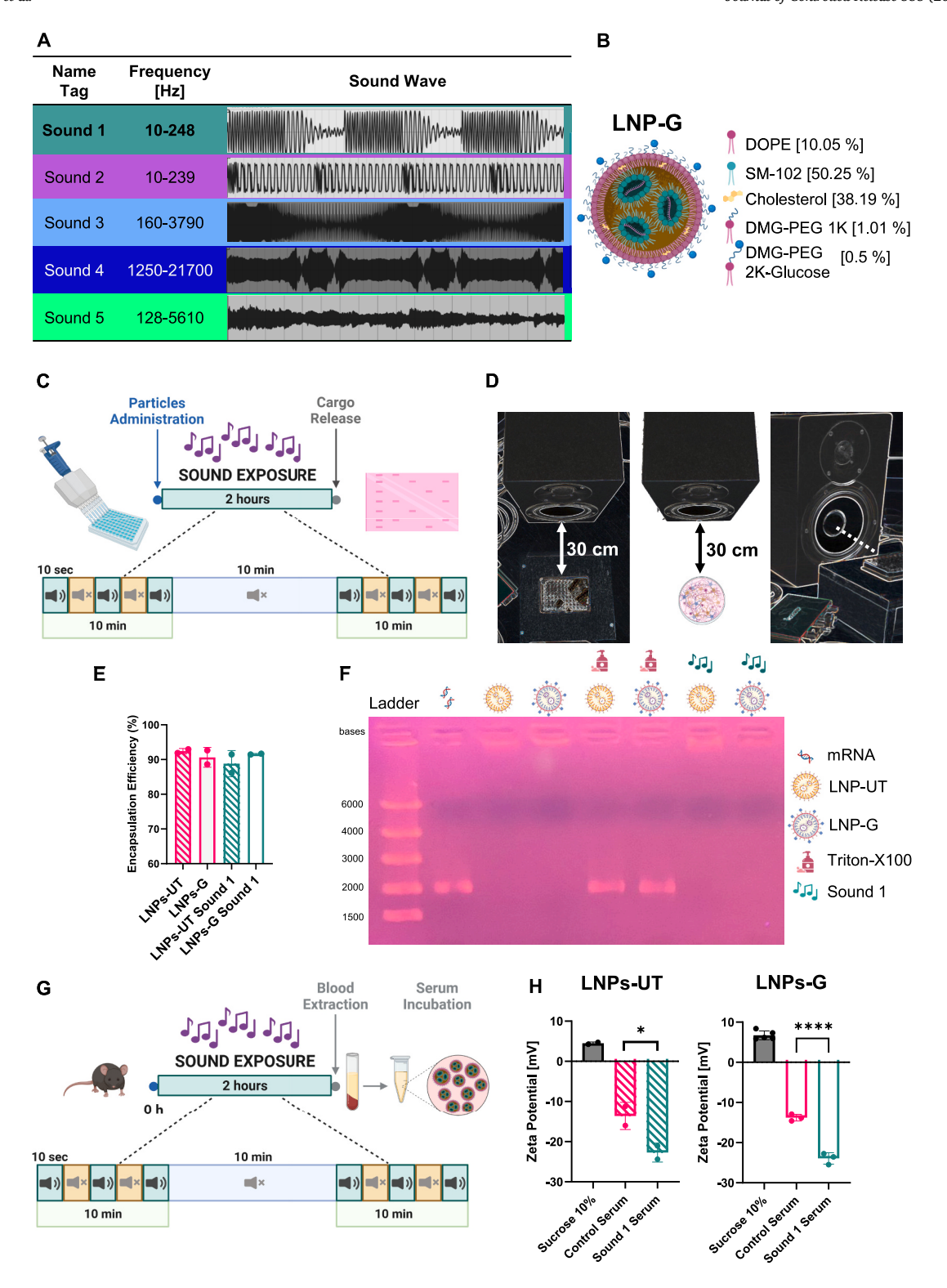


Fig. 1. Impact of sound on LNP stability, cargo release and surface charge. (A) Sound properties and description. (B) Graphic representation of LNPs structure and composition (C) Schematic description of the cargo release experiment. LNPs were exposed to sound for 2 h in 10 min intervals with 10 s intermittent pulses. After, encapsulation efficiency and agarose gel electrophoresis were performed. (D) Experimental set-up. Plates were located 30 cm from the sound reproduction system and elevated to align with the woofer. (E) Sound exposure does not modify encapsulation efficiency of the LNPs as tested by Quant-iT RiboGreen RNA Assay. (F) LNPs do not release mRNA cargo in response to sound exposure. Agarose gel electrophoresis (1 %) shows mRNA bands only when LNPs are disrupted by Triton-X100. (G) Schematic description of sound exposed blood serum incubation experiment. After 2 h of sound exposure, mice were sacrificed and blood extracted. Serum was obtained and LNPs were incubated in two different serums, one from mice exposed to sound and one from unexposed. (H) Serum from sound-exposed mice induced stronger reduction of zeta potential in both untargeted (LNPs-UT) and glucose-modified LNPs (LNPs-G), suggesting a possible change in serum protein composition. Zeta data are presented as mean \pm SD (n = 2–5). *p < 0.031 ****p < 0.0001. One-way ANOVA with adjusted p-values for multiple comparisons was used for statistical analysis.

organic phase (ethanol) containing ionizable lipid (SM-102; 50.25 mol %), a helper lipid (DOPE; 10.05 mol%), cholesterol (38.19 mol%), and PEG-lipids (DMG-PEG1000; 1.01 mol% and DMG-PEG2000/DMG-PEG2000-glucose; 0.5 mol%) (Fig. 1B, Fig. S2B Supporting Information). The combination of PEG moieties of different lengths is based on our previous findings, which showed that combining PEG2000-moiety conjugated to a brain targeting moiety alongside unconjugated PEG1000 lipids in liposome formulation enhances brain cell uptake, by improving ligand-receptor accessibility [55,56].

We assessed the physical properties of the formulated LNPs to ensure consistency (Fig. S2C Supporting Information). The particle sizes of both untargeted (LNPs-UT) and glucose-modified (LNPs-G) formulations were 108.6 ± 0.98 nm to 114.7 ± 3.1 nm respectively. Polydispersity index (PDI) was 0.08 ± 0.01 and 0.06 ± 0.01 , and zeta potentials in 10% sucrose were 4.47 ± 0.24 mV and 6.7 ± 0.98 mV, indicating that the addition of the targeting moiety did not significantly affect the LNPs' size or charge. We also measured zeta potential before and after incubation in mouse serum. After serum incubation, the zeta potential of both formulations shifted to negative values, -13.605 ± 2.395 mV and -13.786 ± 0.67 mV, reflecting a change in the particle's surface being coated by a protein corona [62]. Both formulations achieved mRNA encapsulation efficiencies of $\sim\!90$ %, highlighting the efficiency of the encapsulation process regardless of the glucose moiety.

4.3. Impact of sound exposure on LNP stability, cargo release and surface properties

The use of audible sound to influence the cargo release from LNPs was studied. More specifically, we tested if audible sound and music induce mRNA release from LNPs. The exposure protocol followed 10 s of sound with 10 s of silence, repeated in 10-min intervals of sound exposure, followed by a 10-min break for a total time of 2 h (Fig. 1C). We chose this exposure protocol to avoid the risk of sensory adaptation, potentially reducing the response over time. This pattern allows cells to reset and respond effectively to each subsequent exposure [63–66]. The fact of exposing the sound in 10-min blocks had the purpose of increasing the possible effect induced by the sound. The experimental subject (glass bottom 96-well plate containing either particles (100 µL, 3.4E+10 particles mL $^{-1}$) or cells (200 μ L media volume)) was placed 30 cm from the speaker and was lifted to be aligned with the lower woofer (Fig. 1D). Following sound exposure, the encapsulation efficiency was measured to confirm the integrity of the LNPs. No significant changes in encapsulation efficiency were observed, indicating that the sound exposure did not compromise the ability of the LNPs to retain their mRNA cargo (Fig. 1E). Additionally, the release of the mRNA cargo from the LNP was evaluated post-sound exposure by agarose gel electrophoresis. The gel images showed the absence of RNA bands, indicating no detectable mRNA release from the LNPs following sound exposure. This result suggests that the low-frequency audible sound alone does release the RNA cargo. In contrast, when Triton X-100, a surfactant known to disaggregate LNPs, was added, RNA was released from the LNP, confirming that the RNA remained encapsulated within the LNPs under sound exposure alone (Fig. 1F). Size measurements taken before and after sound exposure also showed no noticeable differences, further confirming that the structural stability of the LNPs was not affected by sound 1 (FigureS2D Supporting Information). In conclusion, these results demonstrate that low-frequency audible sound, applied in a pulsed pattern, did not induce RNA release from LNPs, nor did it affect the particles' integrity.

This sound exposure protocol, which alternates sound and silence, will be used in the following in vitro and in vivo studies to further explore the effects of sound on LNP dynamics.

To further explore how low-frequency audible sound can influence LNP characteristics, we conducted an experiment to assess whether sound exposure alters mice serum composition and the LNPs zeta potential after incubation. Mice were exposed to Sound 1, following the

same pattern previously described (alternating 10 s of sound with 10 s of silence in 10-min intervals, followed by a 10-min break). After 2 h of exposure, the animals were sacrificed, and blood was collected via cardiac puncture. The blood samples were then centrifuged to isolate the serum, which was used to investigate its impact on the LNPs (Fig. 1G). Particles were incubated with either serum from sound-exposed mice or control serum from non-exposed mice for 15 min. Following incubation, the LNPs were washed with PBS, and their zeta potential was measured in 10 % sucrose solution. The values of zeta potential before and after serum incubation with the different serums can help assess the impact of serum proteins on LNP surface charge. Zeta potentials in sucrose 10 %before incubation were 4.47 \pm 0.24 mV and 6.7 \pm 0.98 mV, for LNPs-UT and LNPs-G respectively. After incubating the particles in control mice serum, the zeta potential measured in sucrose 10 % decreased to negative values -13.605 ± 2.395 mV and -13.786 ± 0.67 mV. Moreover, when the serum used for the incubation was from sound-exposed mice, the value dropped to -22.72 ± 1.68 mV and -23.933 ± 1.149 mV (Fig. 1H). The decreased zeta potential of the LNPs incubated in plasma of mice exposed to music suggests that the protein corona formed on LNPs after incubation with the different serums was distinct in composition. These findings imply that exposure to low-frequency sound may induce the release of specific molecules or proteins into the bloodstream [67], which can influence nanoparticle behaviour in biological environments, including cellular uptake or biodistribution/organ tropism.

4.4. LNPs cellular uptake in vitro: Role of sound exposure and frequency

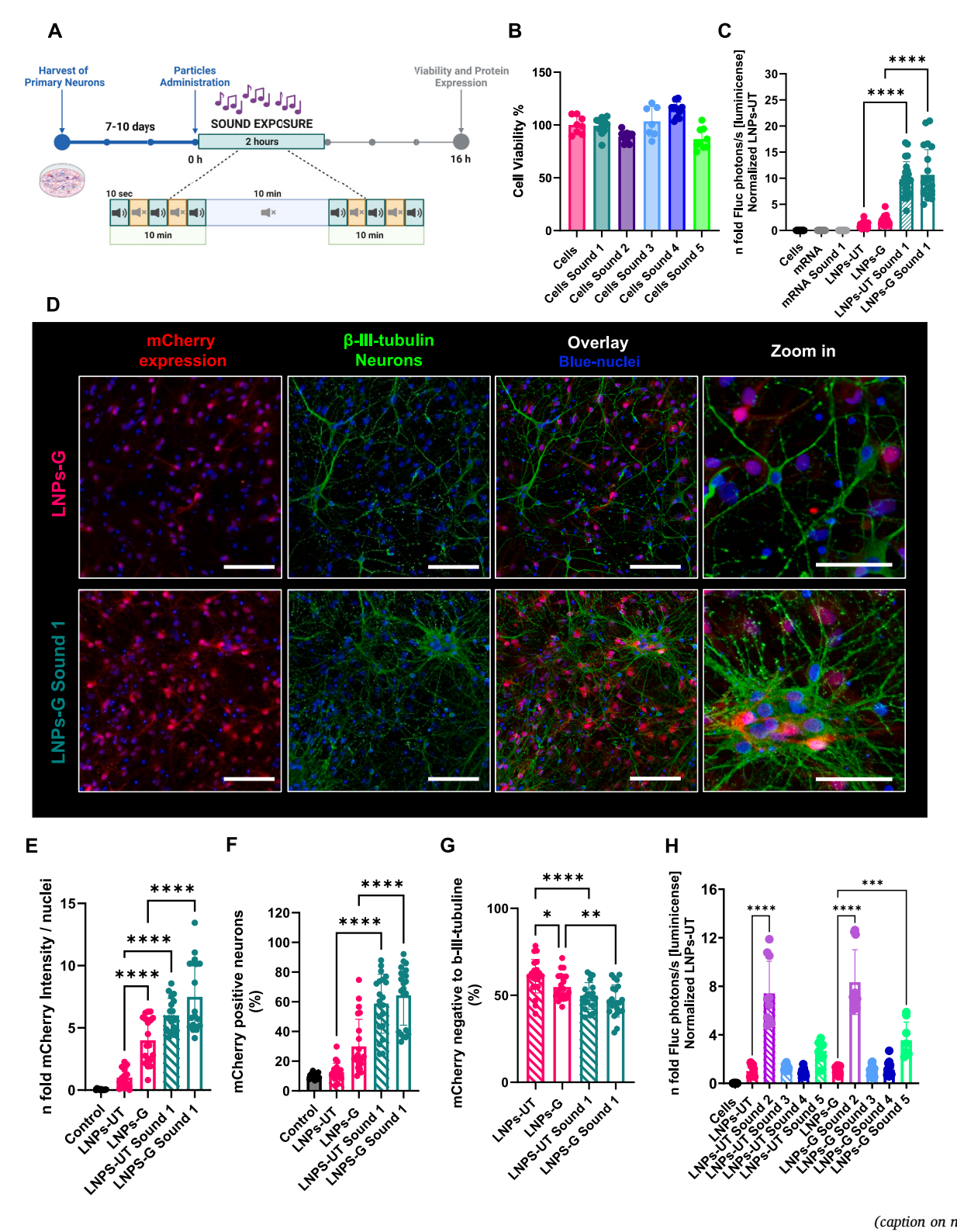
Next, we evaluated the effect of the designed sounds on cell viability across multiple cell lines, followed by an analysis of transfection efficiency (Fig. 2A). Our initial focus was on primary neuron cultures, given their closer relevance to in vivo conditions. Primary neurons were exposed to each sound pattern for 2 h, after which cell viability was measured (Fig. 2B). None of the sound patterns tested reduced cell viability, with all values remaining above 85 % compared to the control neurons that were not exposed to any sound. Following this confirmation of sound safety, we tested cell viability after the addition of various LNP formulations and subsequently exposing the cells to sound. No significant reduction of cell viability was observed (Fig. S3A, Fig. S3B, Fig. S3C, Fig. S3D, Fig. S3E Supporting Information).

To assess transfection efficiency, LNPs were loaded with firefly luciferase (FLuc) mRNA, and primary neurons cells were treated with either the unmodified (UT) or glucose-modified (G) LNP formulations for 16 h, with untreated cells serving as controls (200 ng FLuc mRNA per treatment). Immediately following particle administration, cells were exposed to soundtrack #1 for 2-h, following the previously described sound protocol. After 16 h, luminescence values were measured alongside the previously collected viability values (Fig. 2A). Luminescence data were normalized to cell viability to account for potential differences in cell population per well.

Assessing the effect of glucose modification, the presence of glucose on the surface (LNPs-G) resulted in an increase in neuronal uptake and FLuc mRNA expression (achieving nearly 2-fold higher expression compared to LNPs-UT (Fig. S3F Supporting Information). Importantly, sound #1 exposure further enhanced luminescence. For LNPs-UT, sound 1 exposure increased particle uptake by 9.8-fold, compared to LNPs-UT without sound, while for LNPs-G, sound 1 resulted in an almost 11-fold increase relative to LNPs-UT without sound. This demonstrates the added effect of glucose modification on the LNP surface (Fig. 2C). Results were consistent across two independent experiments in primary neurons culture originally from both male and female rat pups.

Confocal microscopy images were acquired to corroborate the results from the luminescence assay. For this, LNPs were loaded with mCherry mRNA, and cells were treated with either unmodified (UT) or glucose-modified (G) LNP formulations for 24 h, with untreated cells serving as controls (200 ng mCherry mRNA per treatment). Following particle administration, cells were exposed to soundtrack #1 for 2-h to evaluate

its impact on LNP uptake. After 24 h, cells were fixed in 4 % PFA and stained for visualization. Neurons were labelled with β -III-tubulin, a neuronal marker, to identify neuronal uptake specifically within the primary culture (Fig. 2D). Confocal images demonstrated an increase in cellular uptake when the cells were exposed to sound #1. Image analysis showed that, after normalizing mCherry expression to the number or nuclei in each image, sound #1 exposure led to a 6- to 7.5-fold increase in mCherry expression with both LNPs-UT or LNPs-G, respectively (Fig. 2E). Despite the contribution of supporting cells to particle uptake and mRNA expression, the percentage of fluorescence of the neuronal marker β -III-tubulin positive cells for mCherry increased significantly. Further image analysis showed that LNPs-UT achieved a 12 %



(caption on next page)

colocalization of mCherry and β -III-tubulin, which increased to 29 % with glucose-modified particles (LNPs-G), highlighting the impact of active targeting. After sound 1 exposure, the percentage of colocalization (β -III-tubulin-mCherry) from the total β -III-tubulin rose to 58 % with LNPs-UT, and 64 % with LNPs-G (Fig. 2F). Analyzing the data from another perspective, from the total mCherry expression found in the images, 61 % was negative to the neuronal marker β -III-tubulin after LNPs-UT transfection, showing the expression by supporting cells in the culture. This value was reduced to 54 % after conjugating glucose to the surface of the LNP. When cells were exposed to sound #1, these values dropped to 49 % in the case of LNPs-UT and 46 % in the case of LNPs-G (Fig. 2G). These findings underscore that sound exposure not only enhances overall LNP uptake and expression but also specifically increases neuronal uptake.

When assessing transfection efficiency for the other 4 types of sounds designed (Fig. 2H, Fig. 1A, Fig. S1 Supporting Information), soundtracks #2-to-5, only sounds #2 and #5 succeed to significantly increase LNPs uptake or mRNA expression. Sound #2, presenting similar characteristics as sound #1 regarding frequency but different in the consistency of the sound, achieved 7- or 8-fold higher expression with either LNPs-UT or LNPs-G values, respectively. Even though sound #5 achieved significant differences, the capacity of increasing cell uptake and gene expression was significantly lower, reaching only values of 2.5 and 3.5-fold increase, respectively. With the rest of soundtracks, no significant differences were appreciated compared with the LNPs non exposed to sound (Fig. 2H). Therefore, only the sounds that were in the range of 10–250 Hz of frequency or included some of these frequencies in their spectrum succeeded in increasing the uptake of nanoparticles by the primary neuronal culture.

We further evaluated whether the sounds that led to higher transfection efficiency in primary neurons (sounds 1 and 2) had similar effects in other cell lines. For this, LNPs were loaded with firefly luciferase (FLuc) mRNA, and expression was tested in three different cell lines: hCMEC/D3, representing a key component of the BBB basement membrane [68]; differentiated SH-SY5Y cells, which exhibit mature neuronlike phenotypes [69]; and human embryonic kidney cells (HEK293T), widely utilized in biological and biomedical research due to their robustness in protein expression and ease of transfection. All cell lines were treated with LNPs (200 ng FLuc mRNA per treatment) for 16 h or left untreated as controls. Cell viability in all three lines was unaffected by 2-h exposures to sound #1 or #2 (Fig. 3A), and no particle-related toxicity was observed in any of the cell lines as indicated by the consistent number of live cells across all treated groups (Fig. S4A, S4B, S4C Supporting Information). After 16 h, luminescence values were measured and normalized to cell viability as in the previous experiments. The luminescence values in differentiated SH-SY5Y cells and HEK293T, showed no significant differences between non-targeted and glucose-targeted formulations as well as after sound exposure, except for a significant increase in HEKs for LNPs-UT exposed to sound 1 (Fig. 3B, Fig. 3C). When evaluating mCherry mRNA expression in hCMEC/D3

cells by Lionheart FX automated microscope we observed an increase in expression after glucose-targeted formulations treatment, highlighting the importance of glucose targeting for endothelial cells penetrating (Fig. 3D, E). Transfection efficiency values in hCMEC/D3 cells demonstrated that sound 2 significantly increased the uptake and expression of FLuc mRNA, reaching 1.3-fold higher expression in the case of LNPs-UT exposed to sound #2 and 1.6-fold in the case of LNPs-G (Fig. 3F). This demonstrates a distinction in response, with primary neurons being the only tested cell type to exhibit a notable increase in particle uptake and transfection efficiency upon sound exposure, while other cell types showed minimal responsiveness.

We hypothesize that the enhanced particle uptake and transfection efficiency observed in primary neuronal cultures may result from mechanical stimulation of the neurons which leads to increased neuronal activity [23,24]. Mechanical stimulation refers to the physical vibrations generated by low-frequency sound waves, which may directly impact neuronal membranes and neuronal activity. Although neurons are specialized for electrical signaling, the confocal images reveal that mRNA expression is also seen in supportive cells. Sound exposure can influence neurons by inducing activity or modulating their membrane properties, potentially leading to the release of signaling molecules like neurotransmitters or cytokines [67,70,71]. In addition to responding to neuronal signals, neuronal supportive cells may also be directly influenced by sound through mechanosensitive pathways, where vibrations could alter membrane fluidity or activate mechano-responsive pathways, promoting particle internalization [67,72]. The combination of neuronal signaling and the phagocytic nature of supportive stromal cells likely explains the increased uptake seen in these cultures, with stromal cells playing an important role in LNP uptake.

In contrast, other cell lines tested – hCMEC/D3, SH-SY5Y, and HEK293T - lack the capability for neuronal activity. This could explain why either no significant increases or mild increases in particle uptake or transfection efficiency were observed in those cell lines after sound exposure.

To support our hypothesis that sound stimulation enhances neuronal activity and subsequently increases nanoparticle uptake, we designed an experiment utilizing electrical stimulation as a controlled method to modulate neuronal activity. Previous studies have established that electrical stimulation can enhance neuronal excitability and intracellular signaling, which are crucial for effective drug delivery [70,73–78]. Our experimental setup involved stimulating primary neurons at a frequency of 1 Hz with varying amplitudes (80, 120, and 160 mV) following FLuc LNPs administration and after 16 h evaluating the luciferase expression based on the protocol described in Materials and Methods (Fig. S5A Supporting Information). After stimulation, we observed an increase in the uptake of administered LNPs, reaching values of 10.5-fold higher expression when 1-Hz and 80 mV were used, 9.5-fold when the amplitude increased to 120 mV, and 6.5-fold with 160 mV (Fig. S5B Supporting Information). In contrast, when the same stimulation parameters were applied to differentiated SHSY5Y cells -

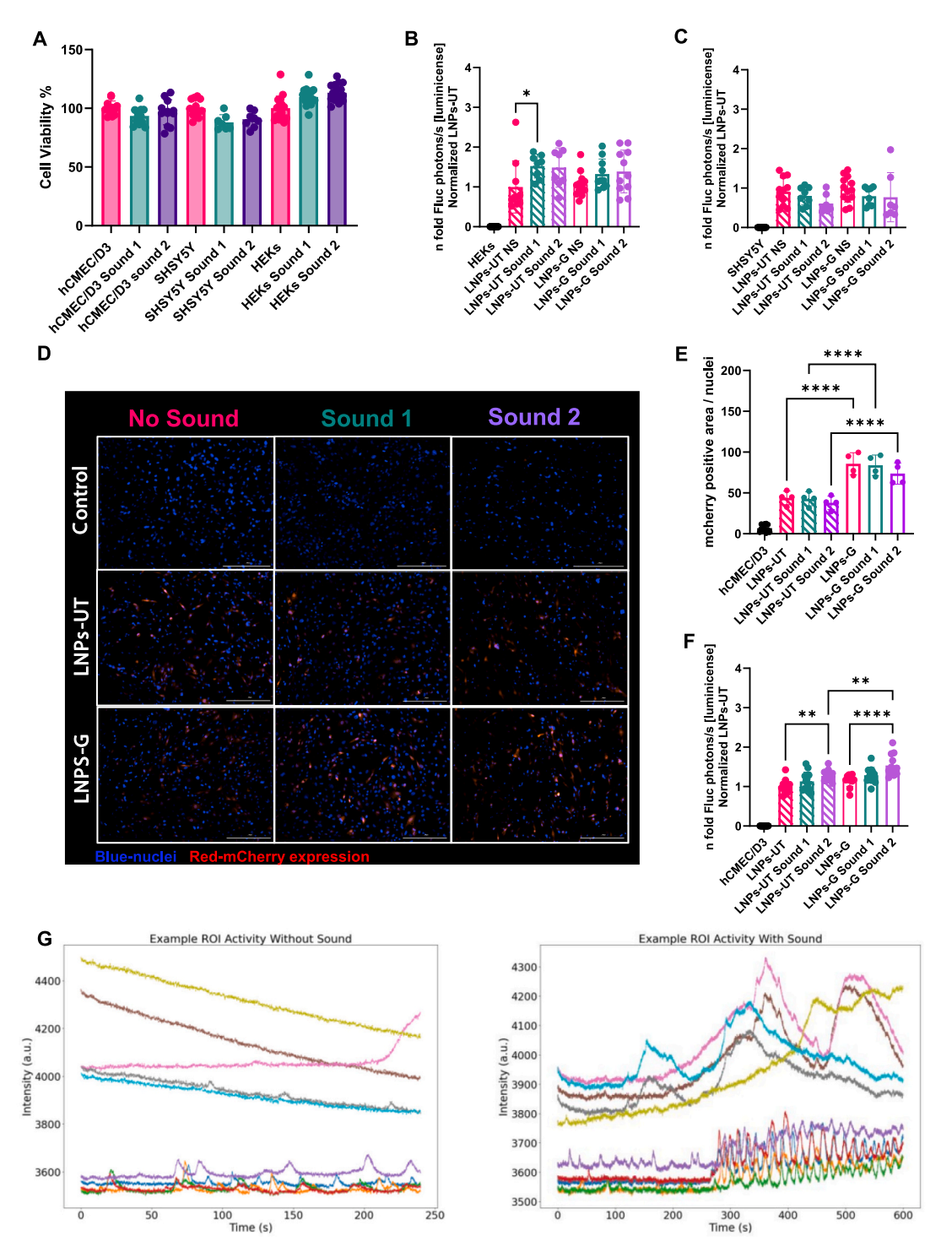


Fig. 3. Cell viability and transfection efficiency in different cell lines. (A) Cell viability of hCMEC/D3, SH-SY5Y and HEK after sound 1 and 2 exposure. (B, C) LNPs transfection efficiency in (B) HEK and (C) SH-SY5Y cells after exposure to sounds 1 or 2. Cells treated with different LNPs but not exposed to sound were used as control. No significant differences were observed in most cases, LNPs-UT exposed to sound 1 in HEK cells showed a significant increase in protein expression. (D) Microscopy images of hCMEC/D3. mCherry expression 24 h after LNPs administration. mCherry (red), nuclei (blue) (scale bar 200 μm) (E) mCherry expression normalized to nuclei number. Sound exposure does not increase the amount of mCherry expression. Data was obtained from image analysis of representative image (n = 4 independent wells per group). (F) LNPs transfection efficiency in hCMEC/D3 cells after exposure to sounds 1 or 2. Cells treated with LNPs (UT/G) but non exposed to sound were used as control. No significant differences were observed after sound 1 exposure. Sound 2 resulted in a significant increase in mRNA expression (< 1.6-fold). (G) Representative Time Series Traces of ROIs with and without Sound Stimulation. The left panel shows activity "Before Sound" and right panel "During Sound" from the same area. The x-axis represents time (seconds), and the y-axis indicates raw fluorescence intensity. Data in each graph are normalized to the corresponding LNPs-UT without sound exposure (n = 8-12). *p < 0.005; ****p < 0.005; ****p < 0.0001. Results are presented as mean ± SD; n represents the number of independent repetitions per group. One-way ANOVA with adjusted p-values for multiple comparisons was used for statistical analysis. (For interpretation of the references to colour in this figure legend, the reader is referred to the web version of this article.)

known to lack the capacity for action potential generation - we did not observe a similar enhancement in LNP uptake (Fig. S5C Supporting Information). This discrepancy highlights the role of neuronal activity in mediating nanoparticle internalization and reinforces our hypothesis regarding the potential of sound exposure to similarly enhance particle uptake through induced neuronal activity. Furthermore, we evaluated the neuronal activity of primary neurons exposed to sound by calcium imaging analysis. The neurons were exposed to three experimental conditions: (1) Before Sound, (2) During Sound, and (3) After Sound. For sound stimulation, sound was applied for 10 min, in intervals of 10 s of sound followed by 10 s of silence. We analysed several metrics (peak frequency, area under the curve and fraction of active time), which allowed us to quantify the frequency, magnitude, and duration of calcium signaling events, providing a comprehensive assessment of neuronal activity under each experimental condition (Fig. 3G, Fig. S6A, S6B, S6C Supporting Information). In addition, a video showed calcium imaging recordings of neuronal activity in the same neuronal culture under two conditions, displayed side by side. The left panel shows the culture in a baseline, unstimulated state, while the right panel depicts the culture following 5 min of sound stimulation (note: the initial 5 min of stimulation are not included in the video). Fluorescence intensity changes, reflecting intracellular calcium transients, serve as a proxy for neuronal activity. A marked increase in activity is observed in the soundstimulated culture compared to the unstimulated condition, illustrating the modulation of neuronal network dynamics by auditory stimulation (Video 1 Supporting Information).

4.5. Proteomic insights into sound-induced modulation of brain microenvironment and nanoparticle uptake

To investigate how sound exposure affects plasma protein composition, plasma samples from control and sound-exposed mice were analysed using the Nano-Omics pipeline [47–50]. The Venn diagram (Fig. S7A Supporting Information) illustrates the common and unique proteins identified in each group, showing an overall overlap in protein composition with some distinct differences. Principal component analysis (PCA) (Fig. S7B Supporting Information) indicated a shift in protein expression patterns between the two groups, with PC1 accounting for 32.4 % of the variance and PC2 for 20.1 %. The clustering pattern suggests a distinct distribution in the Sound #1-exposed group compared to the control.

Differential abundance analysis identified 87 differentially abundant proteins (DAPs) between the groups (Fig. S7C Supporting Information), with 47 upregulated and 40 downregulated proteins in the Sound 1-exposed group. Among these, 20 proteins exhibited a more pronounced difference (p-value <0.01 and log2 fold change >1).

To explore the biological relevance of the above-identified DAPs, Ingenuity Pathway Analysis (IPA) was performed. The top 10 enriched pathways (Fig. S7D Supporting Information) were ranked by p-value, with RhoGDI signaling and actin cytoskeleton regulation among the most significant. The RhoGDI signaling pathway is particularly relevant, as it regulates Rho GTPases, which are essential for maintaining the actin cytoskeleton and stabilizing tight junctions in endothelial cells, including those of the BBB. These findings suggest that sound exposure may influence cytoskeletal organization and endothelial function. To further explore key biological mediators affected by music exposure, network analysis (Fig. S7E Supporting Information) mapped the top five enriched pathways, providing a visual representation of the key proteins involved in these regulatory processes. Overall, the observed differences in plasma composition and associated pathway enrichment indicate biologically relevant shifts in the plasma proteome between the two groups, particularly in pathways related to cytoskeletal integrity and cellular signaling. A table detailing all the specific proteins either downregulated (Table S1 Supporting Information) or upregulated (Table S2 Supporting Information) is provided in the Supporting Information.

Notably, RhoGDI proteins function as negative regulators of Rho GTPases, which are central to cytoskeletal dynamics, cell adhesion, and tight junction maintenance [79]. Reduced RhoGDI signaling may therefore facilitate cytoskeletal remodeling and loosening of tight junctions in the BBB, increasing paracellular permeability. Concurrently, the upregulation of actin cytoskeleton regulators suggests an enhancement of vesicle trafficking and membrane dynamics, potentially increasing cellular predisposition to both endocytosis and exocytosis [80]. Together, these proteomic changes may not only facilitate nanoparticle entry through the BBB and support more effective intracellular processing and transcytosis, particularly in cell types involved in neuronal activation and support [79,81].

4.6. Enhancement of brain uptake and regional distribution of LNPs via sound exposure in vivo

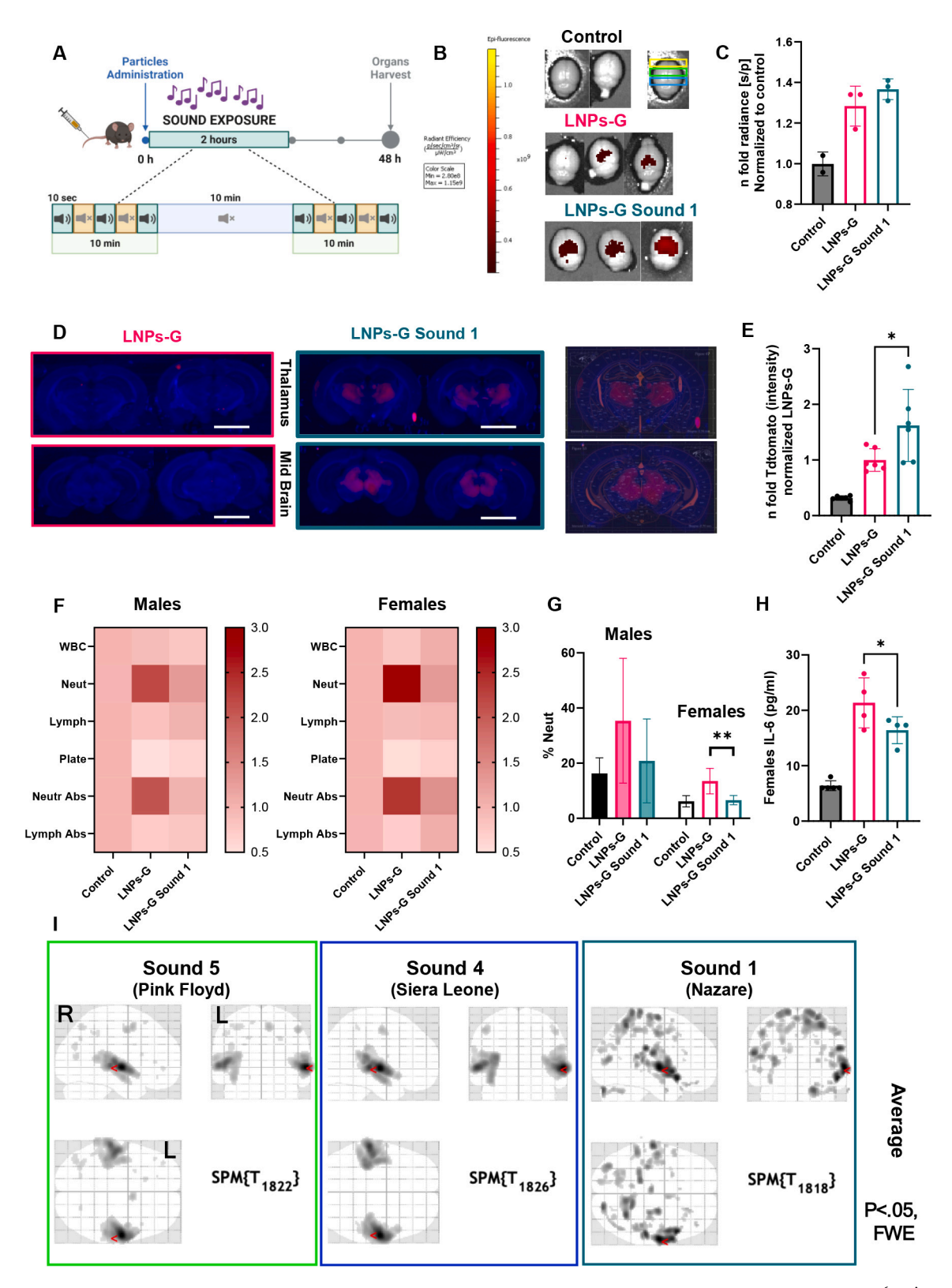
To assess the ability of sound to influence LNP brain uptake and gene expression, we used genetically engineered tdTomato reporter mice (Ai9). These mice are genetically modified to include a LoxP-flanked stop sequence, which blocks the production of the tdTomato protein until Cre recombinase is introduced [82]. When Cre-recombinase is present, the stop sequence is enzymatically removed, enabling tdTomato expression [83]. To apply this model in our system, we intravenously administered LNPs loaded with Cre recombinase mRNA (1 mg/kg Cre mRNA). Immediately after LNP administration, the mice were exposed to sound 1 for 2 h, following the same protocol used in our in vitro studies. Two days later, the mice were perfused and sacrificed, and the brain tissues were harvested (Fig. 4A).

The organs were imaged ex-vivo to evaluate the particles' biodistribution, showing predominant expression in the liver, as is commonly observed in LNPs (Fig. S8A, S8B Supporting Information). The brains were imaged ex vivo to assess the radiance generated by tdTomato expression. Initial comparisons between the control group (untreated), the LNP-G group, and the LNP-G group exposed to sound 1 revealed no significant differences in overall radiance after sound exposure. However, IVIS imaging may not be sensitive enough to resolve intra-brain localization differences (Fig. 4B and C). This result aligns with our in vitro studies, where sound #1 highly improved uptake in primary neuronal cultures but did not affect hCMEC/D3 cells, which are endothelial cells derived from the BBB. These endothelial cells could act as a bottleneck in the delivery approach, limiting the number of particles that reach the brain tissue. Additionally, understanding the mechanisms by which sound influences different cell types at the molecular level might provide insights into how to overcome the limitations posed by endothelial cells at the BBB.

To further examine tdTomato expression resulting from LNP distribution in the brain and given the limited sensitivity of the whole-brain imaging, frozen brain sections covering the main brain areas were processed for detailed analysis. Fluorescent microscopy revealed that while overall tdTomato expression was modest (Fig. S9 Supporting Information), specific regions, particularly the midbrain and thalamus, displayed notably higher expression in mice exposed to sound #1 (Fig. 4D and E). This regional enrichment is consistent with the known roles of these areas in sound processing and emotion regulation [84-86], which are affected by auditory stimulation. The thalamus, specifically the medial geniculate nucleus [87], and the midbrain, particularly the inferior colliculus [88], are central hubs in auditory processing with several functions, including the analysis of the sound frequency and intensity. When mice are exposed to sound, neurons in these regions become more active due to the need for sound processing as well as the mechanical stimulation induced by the sound wave itself, leading to increased neuronal firing. This increased activity could induce changes in membrane permeability or trigger signaling pathways that enhance the uptake of LNPs. The increased cellular activity in response to sound creates a more favorable environment for LNP internalization, particularly by neurons and supportive cells in these sound-responsive regions.

However, the sound frequency used was out of the mouse's hearing range (1–100 kHz) suggesting the impact of the mechanical stimulation achieved by the low-frequency sound. In addition to its role in sound processing, the midbrain's periaqueductal gray (PAG), a region involved in the regulation of fear and emotions [89], could further explain the higher accumulation of particles observed in the midbrain and

thalamus. The PAG is a critical center for controlling defensive responses and is closely connected to the limbic system, particularly in modulating emotional reactions such as fear and anxiety [90]. Exposure to sound, particularly certain types of sound or frequencies associated with emotional responses, may activate these emotional centers, influence the local cellular environment and affect nanoparticles uptake.



(caption on next page)

Fig. 4. Sound increases brain LNP uptake and affects regional brain distribution. (A) Schematic representation of sound effects on LNPs distribution after intravenous administration in vivo. (B, C) Biodistribution in the brain 48 h post-administration of Cre-mRNA loaded LNPs, analysed using (B) an in vivo imaging system (IVIS) and (C) quantified by IVIS software analysis. (D, E) While tdTomato expression (red) remained low, the regional specificity observed in the midbrain and thalamus suggests that sound exposure could enhance LNP uptake and mRNA expression in brain regions associated with auditory processing and sensory integration (scale bar: 5000 µm). (F) Assessment of white blood cell count (WBC) using blood samples collected 48 h after LNPs administration. Differences can be observed between the LNPs-G and LNPs-G Sound 1 specifically in the percentage of neutrophils (Neut) in the sample or the absolute count of neutrophils (Neut abs). A higher reduction in platelets (Plate) can also be appreciated in the case of LNPs-G. All values are normalized to the non-injected control group. Lymph = lymphocytes. (G) Percentage of neutrophils in mice blood samples after LNPs-G administration with or without sound exposure. Sound 1 exposure induces a reduction in the neutrophils % both in males and females after LNPs-G administration. (H) Interleukin (IL)-6 blood serum levels after LNPs-G administration and sound exposure in female mice. Sound exposure significantly reduces the levels of IL-6 48 h after LNPs systemic injection. (I) Functional MRI activation maps (p < 0.05, FWE-corrected) showing brain responses to three distinct auditory stimuli. The analysis demonstrated that Sound 1 induced a broader and more widespread brain activation pattern compared to the other two auditory conditions. The results of C (3 independent repetitions) are presented as mean \pm standard deviation (SD). One-way ANOVA was used for statistical analysis; p value = 0.23. The results of E (6 brain sections replicates) are presented as mean \pm SD. One-way ANOVA was used for statistical analysis; *p < 0.015. The results of F, and G are five independent replicates (n = 5). Results in F are shown as heat maps. One-way ANOVA was used for statistical analysis; *p < 0.0028. The results of H (n=4) are presented as mean \pm SD. One-way ANOVA was used for statistical analysis; * $p \le 0.035$. The results of I (n=4) are presented as mean. (For interpretation of the references to colour in this figure legend, the reader is referred to the web version of this article.)

Furthermore, sound exposure may increase regional blood flow and vascular permeability in the thalamus and midbrain, facilitating greater LNP uptake and gene expression in these areas [29].

While overall tdTomato expression remained low, the regional specificity observed in the midbrain and thalamus (regions closely associated with auditory processing) suggests that sound exposure could enhance LNP uptake and mRNA expression by a potential synergy between two mechanisms, where the physical effects of sound waves complement the biological responses to auditory stimuli, amplifying their impact on nanoparticle delivery. These findings indicate a potential role for sound in modulating the distribution and activity of intravenously administered LNPs within the brain.

4.7. Modulation of inflammatory responses to LNPs by sound exposure

LNP may induce activation of inflammatory and immune responses [39]. To address this challenge, we investigated whether sound exposure could modulate the immune response following LNP administration in male and female mice due to their possible different immune reaction. Mice (mixed population) were intravenously injected with Cre mRNA-LNPs-G and immediately exposed to soundtrack #1 for 2 h. After 48 h, the mice were sacrificed, and blood samples were collected for further analysis. To assess systemic immunogenicity or inflammation, a complete blood count (CBC) and ELISA cytokine test were conducted, with all values normalized to a healthy control group. CBC analysis revealed a notable increase in both the percentage and absolute count of neutrophils following LNPs-G administration. However, in mice exposed to music immediately after LNPs injection, neutrophil levels returned to values close to the untreated control group in both male and female mice (Fig. 4F). Interestingly, male mice displayed higher baseline neutrophil levels than females [91], though the reduction following music exposure was consistent in both sexes (Fig. 4G). When analyzing each parameter in more detail, the percentage of neutrophils differed significantly between LNPs-G administration with, and without, sound exposure, both when populations were pooled together and when males and females were calculated separately (Fig. S10A, S10D, S10G Supporting Information). The percentage of lymphocytes was significantly different when combining both populations as well as in females (Fig. S10B, S10E, S10H Supporting Information). In the case of platelets, there was a significant difference between LNPs-G exposed and non-exposed to sound in males. However, no significant difference was found in females or both genders combined. (Fig. S10C, S10F, S10I Supporting Information). These findings suggest that music may mitigate the immunogenic response triggered by LNPs, as similarly shown in COVID-19 patients, chronically ill or post-operative patients [33,92,93].

When analyzing the inflammatory cytokines IL-6 and IL-1 β through ELISA, several important observations were made. Firstly, for IL-6, significant differences were observed between female mice administered LNPs-G and those exposed to sound (Fig. 4H). However, when

comparing males or combined male and female groups, no significant differences were found, which may be attributed to the timing of cytokine peaks (Fig. S10J, S10K Supporting Information). Cytokine levels, including IL-6 and IL-1 β , typically rise within hours of LNP administration, often peaking between 6 and 24 h, [40,41], then declining within 24 to 48 h. Since our samples were collected after 48 h, interleukin levels may have already decreased. When evaluating IL-1 β levels, the values were consistently below 7.2 pg/mL, which is the detection limit of the ELISA kit (Fig. S11A - S11C Supporting Information), which again can be explained by the timing of sample collection. However, the elevation in neutrophil levels can persist beyond the peak cytokine response, as IL-6 and IL-1 β continue to stimulate neutrophil production and release from the bone marrow [41]. This prolonged effect may explain the observed differences in neutrophil counts.

4.8. Sound-dependent modulation of brain activity revealed by fMRI

To aim for future clinical translation, we examined the effect of the soundtracks on human brain activity. Human volunteers were exposed to three distinct auditory stimuli (Soundtrack #1, 4 and 5) during separate fMRI runs, each presented in randomized order using a block design. Each run consisted of five 30-s sound segments alternating with 30-s silent control periods, with stimuli delivered via noise-attenuating earplugs that ensured high-fidelity transmission inside the scanner environment (Fig. S12 Supporting Information). fMRI analysis revealed that Sound 1 (low-frequency: 10-248 Hz) induced a more widespread cortical activation (frontal, temporal and visual brain regions) compared to the other two auditory conditions (Fig. 4I and Fig. S13 Supporting Information). While the Pink Floyd (Soundtrack #5) and Sierra Leone (Sound #4) stimuli primarily activated the bilateral temporal lobes, consistent with typical auditory processing regions, the Nazareth (Sound #1) stimuli additionally recruited areas in the frontal cortex and occipital lobes, indicating engagement of higher-order associative and possibly multisensory networks. This broader pattern of activation may reflect the capacity of low-frequency sound to induce more integrative neural responses, potentially involving attention, sensorimotor integration, or auditory-visual association (Table S3 Supporting Information). Notably, due to the delivery method used in the fMRI setup using earphones, the physical vibrations associated with low-frequency sound in the in vivo experiments were absent, potentially leading to an underestimation of the full neuromodulatory effects observed during whole-body sound exposure.

These findings parallel our in vivo results in mice, where low-frequency sound exposure (Sound 1) was associated with increased brain uptake of lipid nanoparticles, particularly in deep brain regions such as the midbrain and thalamus. The overlap between the activated areas in the human fMRI and the regions of enhanced accumulation in mice suggests that low-frequency auditory stimulation may modulate brain-wide neural dynamics, creating conditions favorable for

nanoparticle distribution and cellular uptake.

5. Conclusions

Effective delivery of therapeutic agents to the brain remains an unmet clinical challenge. LNPs offer a promising vehicle for drug and gene delivery but enhancing their brain uptake and minimizing inflammatory responses are crucial for improving therapeutic outcomes. Our study demonstrated that low-frequency audible sound (10–250 Hz) exposure achieved a 10-fold increase in gene expression in primary neuronal culture and a 64 % colocalization of transfected protein expression with neuronal markers. This increased uptake in neuronal culture may be related to elevated neuronal activity caused by the mechanical stimulation produced by the low frequency sound wave. Furthermore, the same sound exposure successfully localized the brain transfection to the midbrain and thalamus in mice, regions strongly associated with sound processing and emotional regulation. Supporting this, fMRI analysis in human participants revealed that low-frequency sound stimuli activated a broader network of brain regions, including frontal and occipital areas beyond the auditory cortex, suggesting systemic neural engagement. This suggests a potential synergy between two mechanisms, the physical effects of sound waves inducing mechanical stimulation and the biological responses to auditory stimuli, increasing the impact of sound on nanoparticle delivery. These findings indicate that audible sound could be a valuable tool for enhancing LNPs delivery to specific brain areas.

Moreover, the exposure to low-frequency sound (10-250 Hz) for 2 h immediately after LNP administration reduced circulating neutrophils in the blood after 48 h post injection in both males and female mice. By modulating the immune response, sound exposure may help reduce immune responses associated with LNPs administration, improving both safety and efficacy of these delivery systems. While we observed promising results in our models, further research is needed to explore the long-term effects of sound-modulated LNP delivery in vivo and to understand how different types of sound stimuli might influence uptake across various brain regions. Plasma proteomic analysis revealed changes in pathways related to cytoskeletal remodeling and endocytosis, including downregulation of RhoGDI signaling and upregulation of actin-regulatory proteins, suggesting a sound-induced cellular predisposition to uptake. Future studies could further investigate the molecular mechanisms by which sound enhances cellular uptake, fine-tuning sound frequencies for different people, brain regions and cell types. Additionally, combining sound with other methods, such as BBB permeabilizers (focused ultrasound), may further improve delivery efficiency.

Taken together, this preliminary proof of concept suggests that music can improve neuronal LNP uptake as well as localized brain nanoparticle distribution, requiring more fundamental understanding of the role music can play in drug delivery to the brain.

CRediT authorship contribution statement

Patricia Mora-Raimundo: Writing – review & editing, Writing – original draft, Visualization, Validation, Methodology, Investigation, Formal analysis, Data curation, Conceptualization. Alon Gilon: Investigation, Conceptualization. Haim Kadosh: Formal analysis, Investigation, Writing – review & editing. Yuval Richtman: Visualization, Investigation, Formal analysis. Mor Sela: Methodology, Investigation. Shanny Ackerman: Investigation. Gal Chen: Writing – review & editing, Methodology, Investigation. Ravit Abel: Investigation. Shaked Kagan: Investigation. Noga Sharf-Pauker: Investigation. Or Gigi: Investigation. Hanan Abumanhal-Masarweh: Formal analysis, Investigation. Utkarsh Tripathi: Visualization, Investigation, Formal analysis. Malak Saada: Investigation. Aviram Shemen: Investigation, Formal analysis. Daphna Link-Sourani: Investigation. Jeny Shklover: Writing – review & editing. Rola Farah: Investigation. Tzipi Horowitz-

Kraus: Investigation, Supervision. Marilena Hadjidemetriou: Supervision. Kostas Kostarelos: Writing – review & editing. Shani Stern: Investigation. Avi Schroeder: Supervision.

Declaration of generative AI and AI-assisted technologies in the writing process

During the preparation of this work the authors used OpenAI's ChatGPT for language editing. After using this tool, the authors reviewed and edited the content as needed and took full responsibility for the content of the publication.

Funding

This research was funded by the European Union (ERC, Smart Nanoparticles, 101089009). Views and opinions expressed are however those of the author(s) only and do not necessarily reflect those of the European Union or the European Research Council Executive Agency. Neither the European Union nor the granting authority can be held responsible for them. The research was also supported by the ISRAEL SCIENCE FOUNDATION (grant No.1881/21); The support of Louis Family Fund for Targeted Drug Delivery & Personalized Medicine Technologies (ATS #11948) as well as Levinson Family Recruitment Fund (ATS#11647) are gratefully acknowledged. A Mallat Family Foundation Grant; Unger Family Fund and "Diane Sherman prize for medical innovation for a better world" provided further support. We acknowledge the support of ERC-Stg Grant (2 CE-MECP2 No. 101040128) and ISF grant (1384/21). We also acknowledge the support of Zuckerman STEM leadership program, Israel Science Foundation grants - 1994/21 and 3252 /21. Furthermore, the authors would like to acknowledge the Technion's Integrated Cancer Center, Russell Berrie Nanotechnology Institute (RBNI), Lorry I. Lokey Interdisciplinary Center for Life Sciences & Engineering, and Biomedical Core Facility (BCF). Patricia Mora-Raimundo wishes to thank the Azrieli Foundation for a Post-Doctoral Fellowship. Patricia Mora-Raimundo, Mor Sela and Gal Chen thank Teva Pharmaceuticals and NFBI (The National Forum for Bio-Innovators) for supporting their Postdoctoral and Doctoral Fellowships. Gal Chen also wishes to thank the Baroness Ariane de Rothschild Women Doctoral Program from the Rothschild Caesarea Foundation.

Declaration of competing interest

The authors declare that they have no competing interests.

Acknowledgments

The authors thank Dr. Nitsan Dahan and Dr. Yael Lupu-Haber from the Life Sciences and Engineering Infrastructure Center, Emerson Building for Life Sciences, Technion, and Mrs. Maya Holdengreber at the Biomedical Core Facility, Technion. Some illustrations in this paper were created with the assistance of BioRender. Shklover, J. (2025) https://BioRender.com/2wi860g. We acknowledge the use of Open-AI's ChatGPT for language editing. The sound design and synthesis in this research were created using Ableton Live and its associated synthesizers, including Wavetable and Operator. We acknowledge Ableton AG for providing these tools. The authors also thank Prof. Yossi Yovel for his insightful comments.

For the purpose of open access, the authors have applied a CC BY license to any Author Accepted Manuscript (AAM) arising from this submission.

Appendix A. Supplementary data

Supplementary data to this article can be found online at https://doi. org/10.1016/j.jconrel.2025.114301.

Data availability

All the data needed to evaluate the conclusions in the paper are present in the paper and/or the Supplementary Materials. Correspondence and requests for materials should be addressed to AS (avids@technion.ac.il).

References

- [1] V.L. Feigin, T. Vos, E. Nichols, M.O. Owolabi, W.M. Carroll, M. Dichgans, G. Deuschl, P. Parmar, M. Brainin, C. Murray, The global burden of neurological disorders: translating evidence into policy, Lancet Neurol. 19 (3) (2020) 255–265.
- [2] D. Wu, Q. Chen, X. Chen, F. Han, Z. Chen, Y. Wang, The blood-brain barrier: structure, regulation, and drug delivery, Signal Transduct. Target. Ther. 8 (1) (2023) 217.
- [3] Y. Zhou, F. Zhu, Y. Liu, M. Zheng, Y. Wang, D. Zhang, Y. Anraku, Y. Zou, J. Li, H. Wu, X. Pang, W. Tao, O. Shimoni, A.I. Bush, X. Xue, B. Shi, Blood-brain barrier—penetrating siRNA nanomedicine for Alzheimer's disease therapy, Sci. Adv. 6 (41) (2020) eabc7031.
- [4] X. Yang, W. Yang, X. Xia, T. Lei, Z. Yang, W. Jia, Y. Zhou, G. Cheng, H. Gao, Intranasal delivery of BACE1 siRNA and rapamycin by dual targets modified nanoparticles for Alzheimer's disease therapy, Small 18 (30) (2022) e2203182.
- [5] H. Li, Y. Cao, J. Ye, Z. Yang, Q. Chen, X. Liu, B. Zhang, J. Qiao, Q.-S. Tang, H. Yang, J. Li, Z. Shi, Y. Mao, Engineering brain-derived neurotrophic factor mRNA delivery for the treatment of Alzheimer's disease, Chem. Eng. J. (2023).
- [6] D. Jiang, H. Lee, W.M. Pardridge, Plasmid DNA gene therapy of the Niemann-pick C1 mouse with transferrin receptor-targeted Trojan horse liposomes, Sci. Rep. 10 (1) (2020) 13334.
- [7] W.M. Pardridge, Brain gene therapy with Trojan horse lipid nanoparticles, Trends Mol. Med. 29 (5) (2023) 343–353.
- [8] P. Khare, S.X. Edgecomb, C.M. Hamadani, E.E.L. Tanner, S.M. Da, Lipid nanoparticle-mediated drug delivery to the brain, Adv. Drug Deliv. Rev. 197 (2023) 114861.
- [9] H.I. Labouta, R. Langer, P.R. Cullis, O.M. Merkel, M.R. Prausnitz, Y. Gomaa, S. S. Nogueira, T. Kumeria, Role of drug delivery technologies in the success of COVID-19 vaccines: a perspective, Drug Deliv. Transl. Res. 12 (11) (2022) 2581, 2588
- [10] M. Sela, M. Poley, P. Mora-Raimundo, S. Kagan, A. Avital, M. Kaduri, G. Chen, O. Adir, A. Rozencweig, Y. Weiss, O. Sade, Y. Leichtmann-Bardoogo, L. Simchi, S. Aga-Mizrachi, B. Bell, Y. Yeretz-Peretz, A.Z. Or, A. Choudhary, I. Rosh, D. Cordeiro, S. Cohen-Adiv, Y. Berdichevsky, A. Odeh, J. Shklover, J. Shainsky-Roitman, J.E. Schroeder, D. Hershkovitz, P. Hasson, A. Ashkenazi, S. Stern, T. Laviv, A. Ben-Zvi, A. Avital, U. Ashery, B.M. Maoz, A. Schroeder, Brain-targeted liposomes loaded with monoclonal antibodies reduce alpha-Synuclein aggregation and improve behavioral symptoms in Parkinson's disease, Adv. Mater. 35 (51) (2023) e2304654.
- [11] K. Fan, X. Jia, M. Zhou, K. Wang, J. Conde, J. He, J. Tian, X. Yan, Ferritin Nanocarrier traverses the Blood brain barrier and kills glioma, ACS Nano 12 (5) (2018) 4105–4115.
- [12] C.W. Huang, C.P. Chuang, Y.J. Chen, H.Y. Wang, J.J. Lin, C.Y. Huang, K.C. Wei, F. T. Huang, Integrin alpha(2)beta(1)-targeting ferritin nanocarrier traverses the blood-brain barrier for effective glioma chemotherapy, J Nanobiotechnol. 19 (1) (2021) 180.
- [13] I. Karunakaran, G. van Echten-Deckert, Sphingosine 1-phosphate A double edged sword in the brain, Biochim. Biophys. Acta Biomembr. 1859 (9 Pt B) (2017) 1573–1582.
- [14] M.E. Pizzo, E.D. Plowey, N. Khoury, W. Kwan, J. Abettan, S.L. DeVos, C. B. Discenza, T. Earr, D. Joy, M. Lye-Barthel, E. Roche, D. Chan, J.C. Dugas, K. Gadkar, S. Hamann, R. Meisner, J. Sebalusky, A.C. Silva Amaral, I. Becerra, R. Chau, J. Chow, A.J. Clemens, M.S. Dennis, J. Duque, L. Fusaro, J.A. Getz, M. S. Kariolis, D.J. Kim, K.J. Lechtenberg, A.W.-S. Leung, A. Moshkforoush, H. N. Nguyen, E.S. Ojo, E.R. Thomsen, V.O. Torres, P.E. Sanchez, L. Shan, A. P. Silverman, Z.K. Sweeney, H. Solanoy, R. Tong, M.E. Calvert, R.J. Watts, R. G. Thorne, P.H. Weinreb, D.M. Walsh, J.W. Lewcock, T. Bussiere, Y.J.Y., Zuchero, transferrin receptor–targeted anti-amyloid antibody enhances brain delivery and mitigates ARIA, Science 389 (6760) (2025) eads3204.
- [15] A. Abrahao, Y. Meng, M. Llinas, Y. Huang, C. Hamani, T. Mainprize, I. Aubert, C. Heyn, S.E. Black, K. Hynynen, N. Lipsman, L. Zinman, First-in-human trial of blood-brain barrier opening in amyotrophic lateral sclerosis using MR-guided focused ultrasound, Nat. Commun. 10 (1) (2019) 4373.
- [16] N.A. Lapin, K. Gill, B.R. Shah, R. Chopra, Consistent opening of the blood brain barrier using focused ultrasound with constant intravenous infusion of microbubble agent, Sci. Rep. 10 (1) (2020) 16546.
 [17] M. Shumer-Elbaz, N. Ad-El, Y. Chulanova, D. Brier, M. Goldsmith, M. Bismuth,
- [17] M. Shumer-Elbaz, N. Ad-El, Y. Chulanova, D. Brier, M. Goldsmith, M. Bismuth, A. Brosque, R. Gattegno, D. Sher, A. Gutkin, D. Bar-On, D. Friedmann-Morvinski, D. Peer, T. Ilovitsh, Low-frequency ultrasound-mediated blood-brain barrier opening enables non-invasive lipid nanoparticle RNA delivery to glioblastoma, J. Control. Release 385 (2025) 114018.
- [18] A. Dasgupta, M. Liu, T. Ojha, G. Storm, F. Kiessling, T. Lammers, Ultrasound-mediated drug delivery to the brain: principles, progress and prospects, Drug Discov. Today Technol. 20 (2016) 41–48.

- [19] Y. Li, Y. Jiang, L. Lan, X. Ge, R. Cheng, Y. Zhan, G. Chen, L. Shi, R. Wang, N. Zheng, C. Yang, J.X. Cheng, Optically-generated focused ultrasound for noninvasive brain stimulation with ultrahigh precision, Light Sci Appl 11 (1) (2022) 321.
- [20] T.J. Manuel, J. Kusunose, X. Zhan, X. Lv, E. Kang, A. Yang, Z. Xiang, C.F. Caskey, Ultrasound neuromodulation depends on pulse repetition frequency and can modulate inhibitory effects of TTX, Sci. Rep. 10 (1) (2020) 15347.
- [21] S. Yoo, D.R. Mittelstein, R.C. Hurt, J. Lacroix, M.G. Shapiro, Focused ultrasound excites cortical neurons via mechanosensitive calcium accumulation and ion channel amplification, Nat. Commun. 13 (1) (2022) 493.
- [22] H. Estrada, Y. Chen, T. Lemaire, N. Davoudi, A. Özbek, Q. Parduzi, S. Shoham, D. Razansky, Holographic transcranial ultrasound neuromodulation enhances stimulation efficacy by cooperatively recruiting distributed brain circuits, Nat. Biomed. Eng. (2025).
- [23] K.C. Kasuba, A.P. Buccino, J. Bartram, B.M. Gaub, F.J. Fauser, S. Ronchi, S. S. Kumar, S. Geissler, M.M. Nava, A. Hierlemann, D.J. Müller, Mechanical stimulation and electrophysiological monitoring at subcellular resolution reveals differential mechanosensation of neurons within networks, Nat. Nanotechnol. 19 (6) (2024) 825–833.
- [24] R.T. Mihran, S.K. Lineaweaver, F.S. Barnes, H. Wachtel, Effects of pulsed acoustic and mechanical stimuli on the excitability of isolated neuronal and cardiac cells, Appl. Occup. Environ. Hyg. 11 (4) (1996) 271–274.
- [25] C. Alain, A. Moussard, J. Singer, Y. Lee, G.M. Bidelman, S. Moreno, Music and visual art training modulate brain activity in older adults, Front. Neurosci. 13 (2019) 182.
- [26] H. Fukui, K. Toyoshima, Music facilitate the neurogenesis, regeneration and repair of neurons, Med. Hypotheses 71 (5) (2008) 765–769.
- [27] A.Y.R. Kuhlmann, A. de Rooij, M.G.M. Hunink, C.I. De Zeeuw, J. Jeekel, Music affects rodents: a systematic review of experimental research, Front. Behav. Neurosci. 12 (2018) 301.
- [28] M. Popescu, A. Otsuka, A.A. Ioannides, Dynamics of brain activity in motor and frontal cortical areas during music listening: a magnetoencephalographic study, NeuroImage 21 (4) (2004) 1622–1638.
- [29] A.J. Blood, R.J. Zatorre, Intensely pleasurable responses to music correlate with activity in brain regions implicated in reward and emotion, Proc. Natl. Acad. Sci. 98 (20) (2001) 11818–11823.
- [30] S. Finn, D. Fancourt, The biological impact of listening to music in clinical and nonclinical settings: a systematic review, in: The Arts and The Brain - Psychology and Physiology Beyond Pleasure, 2018, pp. 173–200.
- [31] N. Jausovec, K. Habe, The influence of Mozart's sonata K. 448 on brain activity during the performance of spatial rotation and numerical tasks, Brain Topogr. 17 (4) (2005) 207–218.
- [32] V. Menon, D.J. Levitin, The rewards of music listening: response and physiological connectivity of the mesolimbic system, Neuroimage 28 (1) (2005) 175–184.
- [33] J. Saifman, A. Colverson, A. Prem, J. Chomiak, S. Doré, Therapeutic potential of music-based interventions on the stress response and Neuroinflammatory biomarkers in COVID-19: a review, Music. Sci. 6 (2023), 20592043221135808.
- [34] Effect and mechanism of music therapy on neural restoration in patients with epilepsy, Revista Argentina De Clinica, Psicologica 29 (2020) 1493–1499.
- [35] E. Altenmuller, G. Schlaug, Apollo's gift: new aspects of neurologic music therapy, Prog. Brain Res. 217 (2015) 237–252.
- [36] M.J. Machado Sotomayor, V. Arufe-Giráldez, G. Ruíz-Rico, R. Navarro-Patón, Music therapy and Parkinson's disease: a systematic review from 2015-2020, Int. J. Environ. Res. Public Health 18 (21) (2021).
- [37] A.M. Matziorinis, S. Koelsch, The promise of music therapy for Alzheimer's disease: a review, Ann. N. Y. Acad. Sci. 1516 (1) (2022) 11–17.
- [38] C.L. Xu, J.Z. Nao, Y.J. Shen, Y.W. Gong, B. Tan, S. Zhang, K.X. Shen, C.R. Sun, Y. Wang, Z. Chen, Long-term music adjuvant therapy enhances the efficacy of subdose antiepileptic drugs in temporal lobe epilepsy, CNS Neurosci. Ther. 28 (2) (2022) 206–217.
- [39] S.P. Chen, A.K. Blakney, Immune response to the components of lipid nanoparticles for ribonucleic acid therapeutics, Curr. Opin. Biotechnol. 85 (2024) 103049.
- [40] Y. Lee, M. Jeong, J. Park, H. Jung, H. Lee, Immunogenicity of lipid nanoparticles and its impact on the efficacy of mRNA vaccines and therapeutics, Exp. Mol. Med. 55 (10) (2023) 2085–2096.
- [41] S. Ndeupen, Z. Qin, S. Jacobsen, A. Bouteau, H. Estanbouli, B.Z. Igyarto, The mRNA-LNP platform's lipid nanoparticle component used in preclinical vaccine studies is highly inflammatory, iScience 24 (12) (2021) 103479.
- [42] H. Zhang, X. Han, M.G. Alameh, S.J. Shepherd, M.S. Padilla, L. Xue, K. Butowska, D. Weissman, M.J. Mitchell, Rational design of anti-inflammatory lipid nanoparticles for mRNA delivery, J. Biomed. Mater. Res. A 110 (5) (2022) 1101–1108.
- [43] X. Wang, S. Liu, Y. Sun, X. Yu, S.M. Lee, Q. Cheng, T. Wei, J. Gong, J. Robinson, D. Zhang, Preparation of selective organ-targeting (SORT) lipid nanoparticles (LNPs) using multiple technical methods for tissue-specific mRNA delivery, Nat. Protoc. 18 (1) (2023) 265–291.
- [44] S. Kellner, S. Berlin, Rescuing tri-heteromeric NMDA receptor function: the potential of pregnenolone-sulfate in loss-of-function GRIN2B variants, Cell. Mol. Life Sci. 81 (1) (2024) 235.
- [45] S. Zoabi, M. Andreyanov, R. Heinrich, S. Ron, I. Carmi, Y. Gutfreund, S. Berlin, A custom-made AAV1 variant (AAV1-T593K) enables efficient transduction of Japanese quail neurons in vitro and in vivo, Commun Biol 6 (1) (2023) 337.
- [46] U. Tripathi, I. Rosh, R. Ben Ezer, R. Nayak, Y. Hussein, A. Choudhary, J. Djamus, A. Manole, H. Houlden, F.H. Gage, S. Stern, Upregulated ECM genes and increased synaptic activity in Parkinson's human DA neurons with PINK1/PRKN mutations, npj Parkinson's Dis. 10 (1) (2024) 103.

- [47] L. Gardner, K. Kostarelos, P. Mallick, C. Dive, M. Hadjidemetriou, Nano-omics: nanotechnology-based multidimensional harvesting of the blood-circulating cancerome, Nat. Rev. Clin. Oncol. 19 (8) (2022) 551–561.
- [48] M. Hadjidemetriou, J. Rivers-Auty, L. Papafilippou, J. Eales, K.A.B. Kellett, N. M. Hooper, C.B. Lawrence, K. Kostarelos, Nanoparticle-enabled enrichment of longitudinal Blood proteomic fingerprints in Alzheimer's disease, ACS Nano 15 (4) (2021) 7357–7369.
- [49] X. Liu, H. Abmanhal-Masarweh, O. Iwanowytsch, E. Okwelogu, K. Arashvand, K. Karabatsou, P.I. D'Urso, F. Roncaroli, K. Kostarelos, T. Kisby, M. Hadjidemetriou, Plasma-to-tumour tissue integrated proteomics using nanoomics for biomarker discovery in glioblastoma, Nat. Commun. 16 (1) (2025) 3412.
- [50] M. Hadjidemetriou, L. Papafilippou, R.D. Unwin, J. Rogan, A. Clamp, K. Kostarelos, Nano-scavengers for blood biomarker discovery in ovarian carcinoma, Nano Today 34 (2020).
- [51] L. Schoenmaker, D. Witzigmann, J.A. Kulkarni, R. Verbeke, G. Kersten, W. Jiskoot, D.J. Crommelin, mRNA-lipid nanoparticle COVID-19 vaccines: structure and stability, Int. J. Pharm. 601 (2021) 120586.
- [52] X. Hou, T. Zaks, R. Langer, Y. Dong, Lipid nanoparticles for mRNA delivery, Nat. Rev. Mater. 6 (12) (2021) 1078–1094.
- [53] M. Sela, G. Chen, H. Kadosh, T. Kagan, R. Nicola, S. Turutov, Y. Richtman, L. Zhige, M.R. Albalak Menasherov, S. Kagan, T. Schroeder, P. Mora-Raimundo, R. Kablan, E. Egorov, A. Odeh, T. Abu-Raiya, I. Ionita, I. Freilich, G. Kaneti, I. Knani, Y. Arav, Y. Leichtmann-Bardoogo, K. Tadmor, J. Shklover, T. Patriarchi, D. Danino, P. Hasson, U. Ashery, A. Zeisel, B.M. Maoz, T. Laviv, K. Radinsky, A. Schroeder, Alvalidated brain targeted mRNA lipid nanoparticles with neuronal tropism, ACS Nano (2025).
- [54] A.I. Matos, C. Peres, B. Carreira, L.I.F. Moura, R.C. Acúrcio, T. Vogel, E. Wegener, F. Ribeiro, M.B. Afonso, F.M.F. Santos, Á. Martínez-Barriocanal, D. Arango, A. S. Viana, P.M.P. Góis, L.C. Silva, C.M.P. Rodrigues, L. Graca, R. Jordan, R. Satchi-Fainaro, H.F. Florindo, Polyoxazoline-based Nanovaccine synergizes with tumorassociated macrophage targeting and anti-PD-1 immunotherapy against solid tumors, Adv. Sci. 10 (25) (2023).
- [55] M. Sela, M. Poley, P. Mora-Raimundo, S. Kagan, A. Avital, M. Kaduri, G. Chen, O. Adir, A. Rozencweig, Y. Weiss, Brain-targeted liposomes loaded with monoclonal antibodies reduce alpha-synuclein aggregation and improve behavioral symptoms in Parkinson's disease, Adv. Mater. 35 (51) (2023) 2304654.
- [56] M. Kaduri, M. Sela, S. Kagan, M. Poley, H. Abumanhal-Masarweh, P. Mora-Raimundo, A. Ouro, N. Dahan, D. Hershkovitz, J. Shklover, Targeting neurons in the tumor microenvironment with bupivacaine nanoparticles reduces breast cancer progression and metastases, Sci. Adv. 7 (41) (2021) eabj5435.
- [57] E. Álvarez-Benedicto, L. Farbiak, M.M. Ramírez, X. Wang, L.T. Johnson, O. Mian, E. D. Guerrero, D.J. Siegwart, Optimization of phospholipid chemistry for improved lipid nanoparticle (LNP) delivery of messenger RNA (mRNA), Biomater. Sci. 10 (2) (2022) 549–559.
- [58] S.G. Patching, Glucose transporters at the blood-brain barrier: function, regulation and gateways for drug delivery, Mol. Neurobiol. 54 (2) (2017) 1046–1077.
- [59] L. Szablewski, Brain glucose transporters: role in pathogenesis and potential targets for the treatment of Alzheimer's disease, Int. J. Mol. Sci. 22 (15) (2021) 8142.
- [60] H. Wolburg, S. Noell, A. Mack, K. Wolburg-Buchholz, P. Fallier-Becker, Brain endothelial cells and the glio-vascular complex, Cell Tissue Res. 335 (1) (2009) 75–96.
- [61] M. Maeki, S. Uno, A. Niwa, Y. Okada, M. Tokeshi, Microfluidic technologies and devices for lipid nanoparticle-based RNA delivery, J. Control. Release 344 (2022) 80–96.
- [62] M. Hadjidemetriou, Z. Al-Ahmady, K. Kostarelos, Time-evolution of in vivo protein corona onto blood-circulating PEGylated liposomal doxorubicin (DOXIL) nanoparticles, Nanoscale 8 (13) (2016) 6948–6957.
- [63] J. Benda, Neural adaptation, Curr. Biol. 31 (3) (2021) R110-R116.
- [64] R.P. Lawson, J. Aylward, S. White, G. Rees, A striking reduction of simple loudness adaptation in autism, Sci. Rep. 5 (1) (2015) 16157.
- [65] S.G. Solomon, A. Kohn, Moving sensory adaptation beyond suppressive effects in single neurons, Curr. Biol. 24 (20) (2014) R1012–R1022.
- [66] B.D.B. Willmore, A.J. King, Adaptation in auditory processing, Physiol. Rev. 103 (2) (2023) 1025–1058.
- [67] L. Bartel, A. Mosabbir, Possible mechanisms for the effects of sound vibration on human health, Healthcare (Basel) 9 (5) (2021).
- [68] B. Weksler, I.A. Romero, P.-O. Couraud, The hCMEC/D3 cell line as a model of the human blood brain barrier, Fluids Barriers CNS 10 (2013) 1–10.
- [69] M. Encinas, M. Iglesias, Y. Liu, H. Wang, A. Muhaisen, V. Cena, C. Gallego, J. X. Comella, Sequential treatment of SH-SY5Y cells with retinoic acid and brain-

- derived neurotrophic factor gives rise to fully differentiated, neurotrophic factor-dependent, human neuron-like cells, J. Neurochem. 75 (3) (2000) 991–1003.
- [70] P. Khanna, D. Totten, L. Novik, J. Roberts, R.J. Morecraft, K. Ganguly, Low-frequency stimulation enhances ensemble co-firing and dexterity after stroke, Cell 184 (4) (2021) 912–930.e20.
- [71] T. Lenc, P.E. Keller, M. Varlet, S. Nozaradan, Neural tracking of the musical beat is enhanced by low-frequency sounds, Proc. Natl. Acad. Sci. 115 (32) (2018) 8221–8226.
- [72] S. Ramesan, A.R. Rezk, C. Dekiwadia, C. Cortez-Jugo, L.Y. Yeo, Acoustically-mediated intracellular delivery, Nanoscale 10 (27) (2018) 13165–13178.
- [73] W.S. Bang, I. Han, S.A. Mun, J.M. Hwang, S.H. Noh, W. Son, D.C. Cho, B.J. Kim, C. H. Kim, H. Choi, K.T. Kim, Electrical stimulation promotes functional recovery after spinal cord injury by activating endogenous spinal cord-derived neural stem/progenitor cell: an in vitro and in vivo study, Spine J. (2023).
- [74] F.F.F. Garrudo, R.J. Linhardt, F.C. Ferreira, J. Morgado, Designing electrical stimulation platforms for neural cell cultivation using poly(aniline): Camphorsulfonic acid, Polymers (Basel) 15 (12) (2023).
- [75] G.K. Wu, Y. Ardeshirpour, C. Mastracchio, J. Kent, M. Caiola, M. Ye, Amplitudeand frequency-dependent activation of layer II/III neurons by intracortical microstimulation, iScience 26 (11) (2023) 108140.
- [76] K. Yun, I.U. Song, Y.A. Chung, Changes in cerebral glucose metabolism after 3 weeks of noninvasive electrical stimulation of mild cognitive impairment patients, Alzheimer's Res Ther 8 (1) (2016) 49.
- [77] Q. Zhang, S. Beirne, K. Shu, D. Esrafilzadeh, X.F. Huang, G.G. Wallace, Electrical stimulation with a conductive polymer promotes neurite outgrowth and synaptogenesis in primary cortical neurons in 3D, Sci. Rep. 8 (1) (2018) 9855.
- [78] R. Zhu, Z. Sun, C. Li, S. Ramakrishna, K. Chiu, L. He, Electrical stimulation affects neural stem cell fate and function in vitro, Exp. Neurol. 319 (2019) 112963.
- [79] N. Mosaddeghzadeh, M.R. Ahmadian, The RHO family GTPases: mechanisms of regulation and signaling, Cells 10 (7) (2021) 1831.
- [80] Q. Ru, Y. Wang, E. Zhou, L. Chen, Y. Wu, The potential therapeutic roles of rho GTPases in substance dependence, Front. Mol. Neurosci. 16 (2023) 1125277.
- [81] Q. Lu, F.M. Longo, H. Zhou, S.M. Massa, Y.H. Chen, Signaling through rho GTPase pathway as viable drug target, Curr. Med. Chem. 16 (11) (2009) 1355–1365.
- [82] M. Tabebordbar, K. Zhu, J.K. Cheng, W.L. Chew, J.J. Widrick, W.X. Yan, C. Maesner, E.Y. Wu, R. Xiao, F.A. Ran, In vivo gene editing in dystrophic mouse muscle and muscle stem cells, Science 351 (6271) (2016) 407–411.
- [83] B.T. Staahl, M. Benekareddy, C. Coulon-Bainier, A.A. Banfal, S.N. Floor, J.K. Sabo, C. Urnes, G.A. Munares, A. Ghosh, J.A. Doudna, Efficient genome editing in the mouse brain by local delivery of engineered Cas9 ribonucleoprotein complexes, Nat. Biotechnol. 35 (5) (2017) 431–434.
- [84] P.P. Gao, J.W. Zhang, S.-J. Fan, D.H. Sanes, E.X. Wu, Auditory midbrain processing is differentially modulated by auditory and visual cortices: an auditory fMRI study, NeuroImage 123 (2015) 22–32.
- [85] L. Cheng, S.H. Wang, K. Peng, X.M. Liao, Long-term impairment of sound processing in the auditory midbrain by daily short-term exposure to moderate noise, Neural Plast. 2017 (2017) 3026749.
- [86] M.J. Wohlgemuth, C.F. Moss, Midbrain auditory selectivity to natural sounds, Proc. Natl. Acad. Sci. 113 (9) (2016) 2508–2513.
- [87] O.P. Keifer Jr., D.A. Gutman, E.E. Hecht, S.D. Keilholz, K.J. Ressler, A comparative analysis of mouse and human medial geniculate nucleus connectivity: a DTI and anterograde tracing study, Neuroimage 105 (2015) 53–66.
- [88] G. Cabrera, M. Cavelli, C. Lopez, Z. Rodriguez-Servetti, G. Vanini, M.H. Chase, A. Falconi, P. Torterolo, Wakefulness-promoting role of the inferior colliculus, Behav. Brain Res. 256 (2013) 82–94.
- [89] M. Mokhtar, P. Singh, Neuroanatomy, Periaqueductal Gray, StatPearls, StatPearls Publishing Copyright © 2024, StatPearls Publishing LLC, Treasure Island (FL), 2024
- [90] H. Deng, X. Xiao, Z. Wang, Periaqueductal gray neuronal activities underlie different aspects of defensive behaviors, J. Neurosci. 36 (29) (2016) 7580–7588.
- [91] Y. Xie, D. Xie, B. Li, H. Zhao, Gender differences in low-molecular-mass-induced acute lung inflammation in mice, Int. J. Mol. Sci. 22 (1) (2021).
- [92] S.H. Khan, M. Kitsis, D. Golovyan, S. Wang, L.L. Chlan, M. Boustani, B.A. Khan, Effects of music intervention on inflammatory markers in critically ill and postoperative patients: a systematic review of the literature, Heart Lung 47 (5) (2018) 489–496.
- [93] D. Fancourt, A. Ockelford, A. Belai, The psychoneuroimmunological effects of music: a systematic review and a new model, Brain Behav. Immun. 36 (2014) 15–26.